Aquatic productivity, anoxia and sedimentary pigment dynamics in Lake Amsoldingen in the past Millennium

Master thesis

Faculty of Science, University of Bern

handed in by

Sarah Lea Ogi

2024

Supervisors

Prof. Dr. M. Grosjean

Dr. P. Zahajská

Sarah Lea Ogi (18-109-447)
Gantrischstrasse 52
3006 Bern, CH
sarah.ogi@students.unibe.ch
Institute of Geography and Oeschger Centre for Climate Change Research,
University of Bern

Table of Contents

List of figures

Appendix

List of tables

Abstract

Increasing eutrophication and anoxia have been attributed to significant rises in anthropogenic forcings since 1850 AD. However, eutrophication and anoxia can also occur naturally, making it difficult to investigate the different forcings. Records of sedimentary pigments and elemental composition of lake sediments offer the opportunity to reconstruct past changes in productivity, anoxia and pigment composition. Only few studies focusing on productivity, anoxia and sedimentary pigment dynamics during the last millennium were conducted so far. Here, we aimed at closing this gap by analysing a sedimentary record of Lake Amsoldingen, Swiss Plateau, to reconstruct past aquatic productivity, anoxia, and sedimentary pigment dynamics during the last Millennium. The combination of X-ray fluorescence scanning (XRF), hyperspectral imaging (HSI) and high-performance liquid chromatography (HPLC) enabled us to reconstruct these paleolimnological conditions. Measuring 33 HPLC samples, spanning approximately one thousand years, offered a detailed investigation of phytoplankton community compositions. The uppermost 29 cm, reaching back to the year 1951 AD, were dated using the ^{210}Pb dating method. For the rest of the core, the age was approximated assuming constant sedimentation rates. Our findings revealed that productivity and anoxia during the Medieval Climate Anomaly, a pre-industrial warm period, were primarily driven by processes associated with forest cover such as increased erosional inputs and wind-induced mixing. The phytoplankton community was dominated by pigments of species indicative of low trophic lake states and seasonally oxygenated bottom waters. Decreasing temperatures led to an overall reduction in pigment concentrations during the Little Ice Age (LIA). An abrupt increase in pigment abundance in 1968 AD suggested the initiation of strong eutrophication, mainly driven by increased nutrient inputs into the lake. Changes in phytoplankton community indicated a shift towards higher abundance of cyanobacteria and anoxygenic phototrophic bacteria (APB), indicating eutrophic conditions and increased bottom water anoxia. Eutrophication in Lake Amsoldingen is not as strong as found in other Swiss Plateau lakes. This is likely due to local protection measures, indicating the importance of these measures in mitigating anthropogenic impacts on lake ecosystems. Our results further demonstrate that changes in phytoplankton communities were mainly attributed to changes in nutrient inputs and lake mixing, closely linked with anthropogenic impacts such as deforestation and agricultural intensification.

1. Introduction

Lakes are vulnerable ecosystems and are affected by a series of forcing variables. Those variables include anthropogenic impact (e.g. land-use intensification) and climate change (Cohen, 2003; Heino et al., 2021), all of which endanger these important freshwater resources (Jenny et al., 2016). Since 1850 AD, increasing anthropogenic forcings have significantly increased eutrophication and anoxia in lakes (Jenny et al., 2016; Makri et al., 2019). Eutrophication and anoxia, however, can occur naturally, making it difficult to disentangle possible forcings (Jenny et al., 2016). Nonetheless, different causes can be disentangled by investigating past climate and environmental variability. Past conditions can be studied by long-term records of primary productivity, trophic state, and mixing regimes in lakes (Cohen, 2003; Makri et al., 2019).

Primary productivity, trophic state and mixing regimes of lakes are tightly linked together. More intense land use releases more nutrients into lakes. Increased nutrient inputs lead to elevated aquatic productivity in the surface waters (Lee et al., 2016; Vinçon-Leite & Casenave, 2019). Subsequently, algae can change a lake's trophic state. That is, high algal growth leads to shading and inhibits light penetration into deeper water. As photosynthesis depends on light, shade from algal growth limits photosynthesis, and thus depleting bottom waters of oxygen (Cohen, 2003). Hence, excessive nutrient availability can result in eutrophication of lakes, or even anoxia, by facilitating algal growth (Jenny et al., 2016). When productivity is high, more organic matter settles to the lake bottom and decomposes. During decomposition by heterotrophs, oxygen is consumed (Lee et al., 2016); thus, the oxygen available in the bottom water gradually decreases (Cohen, 2003). Furthermore, oxygen depletion can also be driven by increasing temperatures. This is because increasing temperatures accelerate microbial respiration and mineralization of organic matter, both of which require oxygen. Additionally, oxygen solubility decreases as water temperatures rise (Jenny et al., 2016). Aquatic productivity, trophic states and mixing regimes are, therefore, controlled by complex interactions between various forcings such as climate change and human impact.

Past lake primary productivity, trophic state, and mixing regimes can be reconstructed by using the elemental and pigmental composition of lake sediments (Makri et al., 2019). Chloropigments, such as chlorophylls *a*, *b*, *c*, and derivatives can be used to assess past aquatic productivity of a lake (Zander et al., 2022). Pigments associated with anoxygenic phototrophic bacteria (APB) can be used as indicators of changing lake mixing conditions, meromixis and anoxia, as their production is inhibited under oxic conditions and they are sensitive to changing light intensities and vertical mixing (Butz et al., 2016, 2017).

Previous research on eutrophication and anoxia in Swiss Plateau lakes reported that aquatic productivity decreased during the Little Ice Age (LIA) (Makri et al., 2020). The LIA was a cold period that lasted from around 1300 to 1900 AD (Pfister & Wanner, 2021). Prior to the LIA, 800 to 1300 AD, a warm period occurred, called the Medieval Climate Anomaly (MCA) (Pfister & Wanner, 2021). More

recently, strong increases in eutrophication were reported to have occurred in the Swiss Plateau region in the mid-20th century (Makri et al., 2019). Restoration programs to counteract eutrophication were first implemented in Europe during the 1980s. Despite decreasing the nutrient inputs, previous trophic states could not be restored (Jenny et al., 2016).

Lake Amsoldingen is a small lake located on the Swiss Plateau. The lake has previously been investigated by Lotter and Boucherle (1984), who focused on vegetation dynamics and *Cladocera* community compositions. However, little is known about the lake's pigment dynamics, primary productivity and anoxia over the past millennium. Hence, this study mainly focuses on providing a record of aquatic productivity, anoxia and sedimentary pigment dynamics in Lake Amsoldingen during the past millennium. To distinguish between the main causes of eutrophication and anoxia, it is necessary to consider both pre- and post-industrial periods. The last millennium covers the Medieval Climate Anomaly (MCA, 800 to 1300 AD), the Little Ice Age (LIA, 1300 to 1900 AD) (Pfister & Wanner, 2021), as well as the Industrial Period (after 1750 AD) (Hegerl et al., 2019). The last millennium thus provides an ideal time span to disentangle the main drivers.

2. State of research

2.1. Lake mixing, aquatic productivity and anoxia

The mixing regime of a lake is influenced by various factors such as wind and water density. Water density is affected by changes in temperature and the availability of dissolved and suspended solids (Boehrer & Schultze, 2008). As water density is highest at 4 °C, a density profile can establish in response to changing temperatures (Boehrer & Schultze, 2008). Most lakes in temperate climates are dimictic, experiencing two periods of vertical mixing each year during spring and fall. In spring and fall, the water temperature and density are quite homogeneous, enabling vertical lake mixing. However, in summer and winter, thermal stratification can establish (Wetzel, 2001), dividing the water column into the hypolimnion and the epilimnion. The strength of the density gradient between the hypolimnion and the epilimnion thereby determines the stability of stratification (Boehrer & Schultze, 2008). Warmer temperatures in summer lead to surface water warming and the establishment of summer stratification, preventing water mixing between the hypolimnion and the epilimnion. In winter, a reverse temperature gradient can establish, with cold and low density surface waters, resulting in inverse stratification of the water column (Wetzel, 2001).

Not all lakes are holomictic, showing complete mixing throughout the entire water column (Wetzel, 2001). If a lake remains stratified over several years, developing a stable chemocline, the lake is referred to as being meromictic (Cohen, 2003; Sorrel et al., 2021). Stable stratification thereby leads to increased density differences due to higher concentrations of dissolved substances in the bottom waters (Boehrer & Schultze, 2008). This process is further explained in Chapter 2.2.

The lake's mixing regime is linked to aquatic productivity and the development of anoxic conditions. Permanent stratification prevents the mixing of dissolved substances such as nutrients or oxygen, potentially influencing the community composition of lake organisms. The upward transport of nutrients to the epilimnion during mixing enhances aquatic productivity in the photic zone. At the same time, oxygen from the epilimnion is transported to the oxygen-depleted hypolimnion, changing the phytoplankton community in the lake (Boehrer & Schultze, 2008; Cohen, 2003).

2.2. Trophic state changes, aquatic productivity and anoxia

Since 1850 AD, there has been a substantial increase in eutrophication in response to anthropogenic impacts, accelerating aquatic productivity and changing phytoplankton community composition (Jenny et al., 2016; Makri et al., 2019). Eutrophication not only increases aquatic productivity and alters phytoplankton communities but also affects lake bottom water oxygenation (Makri et al., 2019) and is, thereby, tightly linked to the lakes mixing regime. The accelerated growth of algae in the epilimnion reduces light transparency into deeper water. This inhibition of photosynthesis in deeper fields leads to oxygen depleted bottom waters (Cohen, 2003). Furthermore, high aquatic productivity in the epilimnion results in more organic matter that settles to the ground, where it is decomposed. During decomposition, oxygen is consumed, further depleting hypolimnetic water of oxygen (Lee et al., 2016). The density gradient of the lake is thereby further strengthened as the concentration of dissolved substances in the hypolimnion increases (Boehrer & Schultze, 2008).

In anoxic conditions, the decrease in pH can lead to the dissolution of $CaCO_3$ from the sediment to the water column (Shapley et al., 2005), further strengthening stratification (Boehrer & Schultze, 2008). Under anoxic conditions with low pH, redox sensitive elements such as Fe, Mn and S are redissolved from sediments as well (Davies et al., 2015), again contributing to the stabilization of stratification (Boehrer & Schultze, 2008). Water density differences are influenced not only by thermal factors but also by the concentrations of chemical species. Changes in a lake's trophic state can thus affect the mixing regime by altering the stratification of the lake.

2.3. The spread of eutrophication and anoxia in Swiss Plateau lakes

From around 3.5 kBP onwards, initial anthropogenic impacts in the form of human settlements and forest clearance were documented in the Swiss Plateau region (Lotter, 2001; Makri et al., 2020; Tu et al., 2020). In response to increased erosional nutrient inputs linked to forest clearance, aquatic productivity was accelerated (Lotter, 2001; Makri et al., 2020). Deforestation not only contributed to increased aquatic productivity but also led to enhanced wind-induced mixing of lake waters (Makri et al., 2020). The LIA was characterized by reduced aquatic productivity in response to decreasing temperatures (Makri et al., 2020; Tu et al., 2021). Since the 1850s AD, a global increase in anthropogenic forcings has been reported, substantially accelerating eutrophication and anoxia in lakes (Jenny et al., 2016; Makri et al., 2019). In Switzerland, aquatic productivity and anoxia markedly increased during

the 1950s AD in response to intensified agriculture, marking the onset of modern eutrophication (Makri et al., 2019, 2020; Tu et al., 2020, 2021). The onset of modern eutrophication substantially altered phytoplankton community compositions (Makri et al., 2019).

Although restoration measures to reduce P emissions were implemented in Switzerland in the 1980s AD, the recovery of certain lakes has been delayed, and anoxic conditions in hypolimnetic waters have persisted (Makri et al., 2019). In seasonally stratified and deep lakes, anoxic conditions in the hypolimnion result in the dissolution of P from the sediment to the water column, leading to increased nutrient concentrations in the hypolimnion (Tu et al., 2021). This clearly shows that lake ecosystems are influenced not only by climate but also by anthropogenic forcings such as land use intensification and deforestation (Cohen, 2003; Heino et al., 2021). Both climatic and human-induced pressures endanger these important freshwater resources by increasing eutrophication (Jenny et al., 2016). Eutrophication strongly affects the lake ecosystem by altering the water quality of lakes, promoting toxic algal blooms and changing the lake's biodiversity (Tu et al., 2021).

2.4. Sedimentary pigments

Sedimentary pigments offer valuable means to investigate past trophic states, mixing regimes as well as phytoplankton community composition (Leavitt & Hodgson, 2001). Produced by phototrophic organisms (algae, phototrophic bacteria, higher aquatic plants or macrophytes), pigments are often characteristic for certain groups of these organisms (Leavitt, 1993; Leavitt & Hodgson, 2001). As these organisms differ in the pigments they use and in their environmental requirements, pigments can be used as indicators of past environmental conditions under which these organisms existed (Leavitt & Hodgson, 2001).

Pigments are labile substances that easily degrade within the water column and the uppermost sediments. Before pigments are sedimented, they sink to the lake bottom. During this process, most of the pigments are degraded by photo- and chemical oxidation, herbivory or microbial decomposition in the water column (Leavitt, 1993; Leavitt & Hodgson, 2001). After reaching the sediment, pigment degradation is affected by light, temperature and oxygen availability as well as bioturbation (Leavitt, 1993; Leavitt & Hodgson, 2001; Reuss et al., 2005). The stability of pigments depends on the chemical composition of the pigment and varies between groups (Leavitt & Hodgson, 2001; Reuss et al., 2005). Chloropigments are more stable in the water column, whereas carotenoids degrade less rapidly after they are sedimented (Guilizzoni et al., 2002). Even though only a fraction of pigments is preserved, it has been reported that pigment concentrations correlate with total algal biomass. This correlation between algal production and pigment abundance and preservation allows us to use sedimentary pigments as indicators of past changes in aquatic productivity, anoxia, and mixing regimes within individual lakes (Leavitt & Hodgson, 2001; Reuss et al., 2005).

Phototrophs can use light as a source of energy. Pigments are thereby used to capture light from the sun (Blankenship & Hartman, 1998; Zander et al., 2023). Organisms thereby use different pigments to capture distinct wavelengths of light. During this process, oxygenic phototrophs produce oxygen. Anoxygenic phototrophic bacteria (APB), however, do not produce oxygen (Zander et al., 2023). Chloropigments such as chlorophyll *a*, are produced by oxygenic phototrophs such as algae and cyanobacteria (Reuss et al., 2005), typically found in the photic zone where oxygen and light availabilities are high. Therefore, chlorophylls absorb light at a wavelength around 670 nm (Butz et al., 2016; Zander et al., 2022), corresponding to the maximum of the light spectrum in surface waters (Zander et al., 2023). Chloropigments are often used to assess past aquatic productivity, serving as indicators for total algal biomass (Zander et al., 2022). When chlorophyll *a* is degraded, pheophytin *a* and pheophorbide *a* are produced among other coloured and uncoloured degradation products. Pheophorbide *a* can be used as an indicator for zooplankton grazing (Cartaxana et al., 2003).

APB can further be divided into two main groups: the green sulphur bacteria (GSB, *Chlorobiaceae*) and the purple sulphur bacteria (PSB, *Chromatiaceae* and *Ectothiorhodospiraceae*). Instead of chlorophylls, APB use bacteriochlorophyll (BChl) pigments for photosynthesis. Like some oxygenic phototrophs, APB use additional carotenoid pigments to absorb light in a wider light spectrum. PSB produce BChl *a* and the carotenoid okenone (Zander et al., 2023). Bacteriopheophytin *a* (Bphe *a*) is a stable degradation product of BChl *a* and is often preserved in sediments. The production of Bphe *a* is sensitive to changes in light intensities and vertical mixing, and is limited by high oxygen availability. PSB are typically found at or below the chemocline and are often limited by low light availability. PSB are able to tolerate oxygen concentration (Zander et al., 2023) and absorb light at a wavelength of around 845 nm (Butz et al., 2016; Zander et al., 2022). GSB use BChl *c*, *d* or *e* and the carotenoids isorenieratene and chlorobactene. BChl *c*, *d* and *e* absorb light at wavelengths around 710 nm. GSB can persist under conditions where light availability is low and GSB are strictly anaerobic. Thus, they are found further down in the water column than PSB. Pigments associated with APB are diagnostic for permanent stratification and anoxia (Butz et al., 2016, 2017). Since PSB and GSB differ in their oxygen and light requirements, their combined analysis can be used to reconstruct oxygen and light availability in the water column (Zander et al., 2023).

Total carotenoid (TC) concentrations have been shown to significantly correlate with total phosphorus (TP) concentrations in the water column. By using a transfer function, sedimentary TC concentrations can be used to estimate total phosphorus (TP) concentrations in the water column at the time of pigment formation (Guilizzoni et al., 2011). The CD/TC (*chlorophyll derivatives / total carotenoids*) ratio indicates the trophic state of a lake (Swain, 1985). As carotenoid rich cyanobacteria are favoured under eutrophic conditions, a low CD/TC is indicative of these conditions (Guilizzoni & Lami, 2003). As carotenoids are better preserved under anoxic conditions, a low CD/TC ratio further indicates good pigment preservation (Swain, 1985). The Chlorophyll Preservation Index (CPI), defined as

(*chlorophyll a / chlorophyll a + pheopigments a*), is used as a further indicator for pigmen preservation (Buchaca & Catalan, 2008). Good pigment preservation is shown by constant CPI values around 0.2 (Buchaca & Catalan, 2008; Deshpande et al., 2014).

2.5. Aim and research questions

The project was guided by the following research questions:

i. How did aquatic productivity and anoxia in Lake Amsoldingen change during the past millennium and which were the underlying causes?

ii. How does the primary productivity and anoxia history compare between pre-industrial times (before 1750 AD) and the Anthropocene (20th century)?

iii. Do changes in the pigment composition (algal communities) follow a typical succession and can this be interpreted in terms of changes in mixing regimes (nutrient availability)?

To provide a record of aquatic productivity, anoxia and sedimentary pigment dynamics in Lake Amsoldingen during the past millennium, the sediment core AMS22-8 was investigated. To address these research questions, pigments were measured using both Hyperspectral Imaging (HSI) and high-performance liquid chromatography (HPLC). The obtained data was combined with data derived from XRF, LOI and CNS analysis.

The personal goal of this thesis was to gain the technical knowledge required to conduct a paleolimnological research project, more specifically:

1) to acquire the knowledge to perform some of the basic paleolimnological methods and handle the according tools
2) getting experience in High Performance Liquid Chromatography (HPLC)
3) applying statistical methods on the compiled data

3. Study site

Lake Amsoldingen is located on the Swiss Plateau in the Canton of Bern, Switzerland (46°43'30''N, 7°34'30'' E, *Figure 1*). The lake is situated approximately 5 km southwest of the city of Thun and 25 km southeast of the city of Bern. With a length of 1080 m, an average width of 352 m and a surface area of 0.38 km^2, Lake Amsoldingen is relatively small (Lotter & Boucherle, 1984). It reaches a maximum water depth of 14.2 m and the volume of the lake is 2552682 m^3 (Guthruf et al., 2015). At 641 m a.s.l., the site is part of the collin to submontane vegetation belt, a humid region with high precipitation and winter frost (Eicher, 1987). Lake Uebeschi is located approximately 500 m northwest of Lake Amsoldingen (Guthruf et al., 2015). The inflowing creek from Lake Uebeschi (Seemattbach) is the biggest of five inflows. The outflow near the castle runs via Glütschbach into the Aare River (Guthruf et al., 1999).
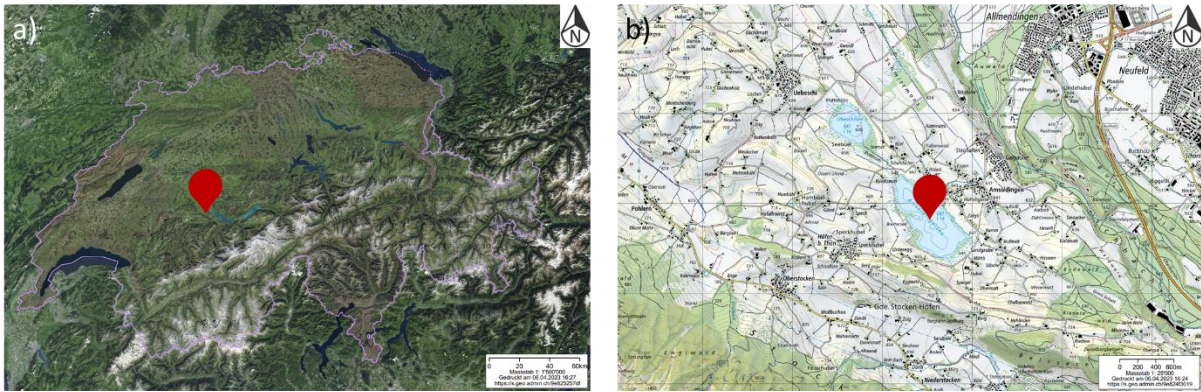
Figure 1: *a) Location of Lake Amsoldingen in Switzerland (red needle, 46°43'30''N, 7°34'30'' E). b) Topographic map of the area around Lake Amsoldingen (Bundesamt für Landestopografie swisstopo, 2023).*

The retreating Aare glacier led to the formation of Lake Amsoldingen. Thereby, the lateral moraine formed a basin that was filled with melt water from the remaining ice (Lotter & Boucherle, 1984). The topographic catchment area spans 4.202 km^2 (Guthruf et al., 2015). *Figure 2* shows a summary of the catchment composition of Lake Amsoldingen. The catchment is mainly characterized by extensive agricultural fields, covering 72% of the area. 13% of the catchment is covered by water. Unproductive land, including vegetation-free areas (debris and rocks) contributes to around 10% of the catchment. Forests and settlements represent only small fractions, making up 3% and 2% of the catchment. In 1977 AD, the "Amsoldingen- und Uebeschisee" nature protection area was established (Guthruf et al., 1999).
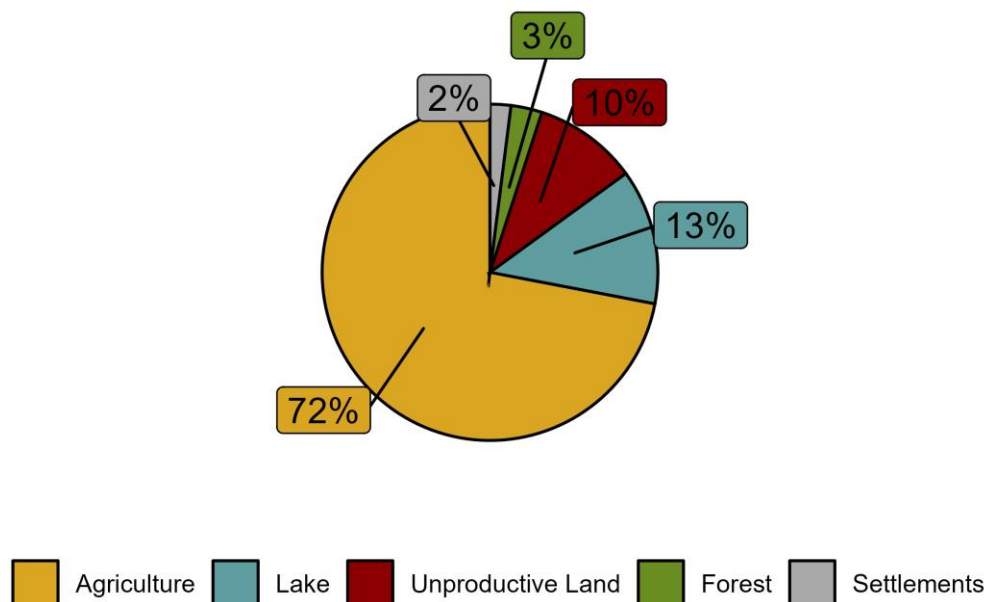
Figure 2: *Composition of the catchment of Lake Amsoldingen, adapted from Guthruf et al. (2015)*

Lake Amsoldingen is a classic paleolimnological site, previously investigated by Lotter and Boucherle (1984). Their study provided information on past trophic lake states. The warming during the Bølling led to increased aquatic productivity and a first occurrence of anoxic conditions (Guthruf et al., 1999; Lotter & Boucherle, 1984). A lowering of the lake level during the Allerød further increased aquatic

productivity, eventually leading to eutrophic conditions (Guthruf et al., 1999; Lotter & Boucherle, 1984). The cooling during the Younger Dryas resulted in decreased aquatic productivity, classifying the lake as oligotrophic. These conditions persisted during the Pre-Boreal period (Guthruf et al., 1999; Lotter & Boucherle, 1984). In the Older Atlantic, aquatic productivity increased, and trophic conditions shifted from oligotrophic to mesotrophic. The first human settlements around Lake Amsoldingen established around 2000 years ago, leading to increased deforestation and the establishment of eutrophic conditions (Lotter & Boucherle, 1984).

The natural trophic state of the lake is mesotrophic but has shifted to current eutrophic conditions. In respect to its mixing regime, the lake can be classified as holomictic and dimictic if the lake freezes in winter (Guthruf et al., 1999). During summer, the lake is stably stratified and thus mixing is inhibited. The decomposition of dead biomass results in oxygen-depleted conditions from a depth of 7 m downwards. When stratification is weakened, the lake water can be mixed. Thereby, the oxygen-depleted hypolimnion is mixed with the oxygen-rich epilimnion (Guthruf et al., 2015).

4. Materials and methods
4.1. Sampling campaign
In October 2022, the Paleolimnology group of the University of Bern cored Lake Amsoldingen. Several sediment cores were retrieved by using either an UWITEC piston corer for long cores or an UVITEC gravity corer for surface cores. For this study, core AMS22-8 (46°43'31.0"N, 007°34'34.4"E) was selected. The core was taken at a water depth of 13.9 m and has a length of 125 cm. The water-sediment interface is undisturbed. We chose the coring location based on its proximity to the deepest point of the lake as the sediment is less disturbed. The cores were stored vertically in the dark at 4 °C in the cold room at the Institute of Geography of the University of Bern. We opened the core by splitting it lengthwise on October 20th, 2022. One half of the core was used for non-destructive analysis (smear slides, XRF and HIS) and for destructive analyses, and the other half for storage.

4.2. Core description and smear slide analysis
We used the classification scheme of Schnurrenberger et al. (2003) to describe the sediment of the core. First, the macroscopic features were assessed visually. The Munsell Soil Colour Chart was used to describe the sediment colour. In a second step, smear slides were used to assess the microscopic features of the sediment. The protocol by LRC, University of Minnesota (Tool of Microscopic Identification (TMI); https://tmi.laccore.umn.edu/, last accessed 20.10.2023) was used to identify different components in the sediment core (organic matter, inorganic matter such as silicates and carbonates). The glass slides were cleaned with deionized water and labelled (AMS22-8, sediment depth). In total, 13 samples were taken every 10 cm starting from a sediment depth of 2.5 cm. We took a little of sediment samples with the tip of a toothpick and smeared it on the slides with the help of a drop of deionised water. After the water evaporated, we added two drops of optical cement (Aquatex 1.08562.0050) to

secure the cover slip. The slides were then examined under a light microscope to classify the most abundant sediment components. Cross-polarized light microscopy was then used to identify minerals such as carbonates. The size of carbonate particles was measured under the microscope to classify the sediment. To estimate diatom abundance and composition, up to 100 diatoms were counted. Thereby, the number of planktonic and benthic diatoms within these 100 counted diatoms was noted. If less than 100 diatoms were present, all diatoms were counted, and percentages calculated. The percentages of microscopic features were estimated for total inorganic matter and total organic matter. All inorganic particles thereby give the percentage of total inorganic matter. Thes same was done for total organic matter. All present *Phacotus sp.* were counted and presented as absolute numbers.

4.3. Dating

The uppermost 29 cm of the core were ^{210}Pb dated at the University of Gdańsk, Poland by the group of Prof. Dr. Wojciech Tylmann, using gamma-spectrometry. The samples were continuously taken at 2 cm intervals. Because of the half-life time of ^{210}Pb of 22.3 years, the dating method can only cover the last 100 to 200 years (Gäggeler & Szidat, 2016). The ^{210}Pb isotope is part of the [238]U decay series in the lithosphere. The intermediate isotope [226]Ra is formed during the decay of [238]U to [222]Rn. The noble gas [222]Rn is released into the atmosphere, where it decays to [210]Pb (Cohen, 2003). The resulting atmospheric ^{210}Pb isotopes are known as unsupported [210]Pb. When ^{210}Pb is sedimented, the unsupported ^{210}Pb decays exponentially with age and can thus be used to date the sediment. [210]Pb can also be produced in situ, when [238]U is sedimented (Gäggeler & Szidat, 2016). The ^{210}Pb coming from the lithosphere is known as supported [210]Pb. The radioactivity of supported ^{210}Pb is in equilibrium with the [226]Ra activity and can thus be estimated by measuring the [226]Ra activity (Cohen, 2003). By subtracting the [226]Ra activity from the total ^{210}Pb activity, the unsupported ^{210}Pb activity can be calculated (*Equation (1)*):

$$A_{unsupported} = A_{total} - A_{supported}$$

(1)

To obtain the according sediment ages, different models can be used. The Constant Rate of Supply (CRS) model assumes constant influx of unsupported ^{210}Pb to the sediment over time. The mass accumulation rate (MAR) is variable. The ^{210}Pb activity at depth x is given by the following equation (*Equation (2),* Swarzenski, 2014):

$$A(x) = A_0^{(-\lambda t)}$$

(2)

$A(x)$ is the unsupported ^{210}Pb activity at a sediment depth x. A_0 is the initial total unsupported ^{210}Pb activity in the sediment core, given by *Equation (3)* (Last & Smol, 2002)*:*

$$A_0 = \left(\frac{^{210}Pb_{unsupported}\ supply\ rate}{sediment\ accumulation\ rate} \right)$$

(3)

λ is the ^{210}Pb decay constant ($0.03114\ year^{-1}$) and t the time. The sediment age at depth x can then be determined by using *Equation (4)* (Swarzenski, 2014):

$$t = \left(\frac{1}{\lambda} \right) In \left[\frac{A_0}{A(x)} \right]$$

(4)

Due to processes such as sediment focusing, erosion or coring, parts of the sediment surface can be lost, decreasing the ^{210}Pb inventory. If the core is not taken at a sufficient length to reach the equilibrium line between unsupported ^{210}Pb and ^{226}Ra, ^{210}Pb activity in the core can be lost. The exponential decrease in ^{210}Pb activity over time causes additional loss as the activity mathematically cannot reach zero. This missing inventory causes systematic inaccuracies in CRS models, resulting in older dates. By using *Equation (5),* the missing inventory can be corrected:

$$A_i = \frac{1}{\lambda}\ r_i C_i$$

(5)

A_i represents the missing inventory, r_i the sediment accumulation rate (SAR) and C_i the unsupported ^{210}Pb right above the depth of the equilibrium line (Tylmann et al., 2014).

To further constrain the CRS model, ^{137}Cs activity measurements were used. The radioisotope ^{137}Cs is created during nuclear fission and does not occur naturally. During nuclear fission, the isotope is released into the atmosphere and can be deposited in lake sediments. Peaks in ^{137}Cs activity at specific sediment depths can be used to match the according depth to a certain nuclear event and thus to a specific time (Last & Smol, 2002; Gäggeler & Szidat, 2016). Nuclear bomb tests started in 1954 AD, indicated by a first peak in ^{137}Cs activity in lake sediments. Right after the nuclear weapon test ban, nuclear fallouts reached their peak in 1962-1963 AD. In Europe, high ^{137}Cs emissions were recorded in 1986 AD, which were caused by the Chernobyl accident (Last & Smol, 2002; Gäggeler & Szidat, 2016).

4.4. X-ray fluorescence scanning (XRF)

X-ray fluorescence scanning is a non-destructive method to determine the elemental composition of sediment cores (Croudace et al., 2019). The split sediment core is exposed to incident X-radiation. Thereby, electrons are ejected from the inner atomic shell. The resulting vacancies are filled by electrons coming from higher-state orbitals in the outer shell to become more stable. During this transition, fluorescence radiation is emitted. The relative abundance of elements in the split core can be estimated

by the energy and wavelength spectra of the emitted fluorescence light, which are specific to atoms of a certain element (Weltje & Tjallingii, 2008). The elemental composition of the sediment core provides important information on environmental changes, including climate change and anthropogenic impacts (Croudace et al., 2019; Davies et al., 2015). The measured elements used in this project are listed in *Table 1*.

The XRF-scanning was done October 20th, 2022, with an ITRAX[TM] XRF Core Scanner at the Institute of Geological Sciences at the University of Bern. We used a Chromium-Anode-Tube which is normally used to measure lighter (low atomic number) elements (Ohlendorf et al., 2015). The instrument operated at a resolution of 0.5 cm, with an integration time of 30 s, running at 30 kV and 50 mA. Every possible element was measured (see Appendix *Figure A1*). In a first step, the elements with very low abundance were excluded (less than 1000 counts per second). Afterwards, the remaining elements (Al, Si, S, K, Ca, Ti, V, Mn, Fe, Ni, Zn, Cu, Mn, Rb, Sr and Sb) were quantitatively analysed. The selected elements were then interpreted in accordance with (Davies et al., 2015):

Table 1: Elements and rations obtained by XRF core scanning used in this project and their interpretation according to Davies et al. (2015)

Elemental indicators	Interpretation
Ca	Calcite precipitation, increased primary productivity
Ti	Increased detrital input
Si/Ti	Increased biogenic silica production often indicative of diatoms
Fe	Detrital input, redox conditions
Mn	Detrital input, oxygenation of bottom waters
Fe/Mn	Reducing conditions
S	Precipitation of Sulphur minerals (Juillot et al., 2023)
Zn	Precipitation of zinc minerals (Juillot et al., 2023)
Inc/Coh	Increased organic content

Because the lowermost 10 cm of the sediment surface was uneven and resulted in implausible data, the analyses were only done for 115 cm of sediment (the complete XRF profiles can be seen in *Figure A1*).

4.5. Hyperspectral Imaging (HSI)

Hyperspectral Imaging (HSI) is used to analyse the sedimental composition of split cores. The sediment of the half core is illuminated by light at visible, and near infrared wavelengths (400 to 1000 nm for the device used in this project). The reflected light on the surface is then recorded by the hyperspectral camera, resulting in spectral reflectance profiles for every pixel. The resolution of the hyperspectral image is thereby given by the distance between sediment surface and camera (Zander et al., 2022). To investigate pigments in the sediment, spectral indices can be used An example for spectral indices are relative absorption band depths (*RABD*), which indicate how different substances (e.g. natural pigments such as chlorophyll *a, b* and *c* and bacteriochlorophylls) influence specific spectral regions. Different substances absorb electromagnetic energy in different spectral regions. These wavelength regions are

known as absorption bands and are indicative for the corresponding substances (Butz et al., 2015, 2016, 2017). $RABD$, however, can be used as indicators but do not provide quantitative measures of pigments (Butz, 2016). Green pigments (chlorophylls) absorb light at wavelengths around 670 nm, indicated as a trough in the reflectance spectra around this wavelength (Butz, 2016; Zander et al., 2022). Thus, $RABD_{673}$ is used as an indicator index for aquatic productivity of green pigments. Bacteriopheophytin a (Bphe a) is indicated by a trough around 845 nm, as it absorbs light around this wavelength. $RABD_{845}$ is used as an indicator for Bphe a (purple sulphur bacteria (PSB)) (Zander et al., 2022, 2023). BChl c, d and e (green sulphur bacteria) absorb light at wavelengths around 710 nm and are indicated by the $RABD_{710}$ index. Sorrel et al. (2021) defined $RABD_{620}$ as an indicator for phycocyanin (cyanobacteria). The indices were calculated according to Zander et al. (2022) which is based on Butz et al. (2015) (*Equation (6)*):

$$RABD_{min} = \frac{\dfrac{X \times R_{Left} + Y \times R_{Right}}{X + Y}}{R_{min}}$$

(6)

Table 2: *List of terms used to calculate the RABD indices as a weighted average of R_{Left} and R_{Right} at the position of R_{min} according to Zander et al. (2022), based on Butz et al. (2015)*

Term	Definition
R_{min}	Trough minimum, lowest reflectance value and highest absorption within R_{Left} and R_{Right}
X	Number of spectral bands between R_{Right} and the trough minimum (R_{min})
Y	Number of spectral bands between the trough minimum (R_{min}) and R_{Left}
R_{Left} and R_{Right}	Endpoint wavelengths: • R_{Left}: reflectance at the start of the absorption feature • R_{Right}: reflectance at the end of the absorption feature

The exact formulas for the indices used in this study were defined based on the endmember spectra and are shown in the appendix (*Equations (A1) – (A4)*). All measured HSI indices are seen in *Figure A3*.

Before the core was scanned, it was left to dry in the dark for two days, as reflectance of the surface was too high to obtain representative data. The core was scanned with a Specim PFD-CL-65-V10E VNIR sediment-core-scanning system (SCS) at the University of Bern. The system was operated at an exposure time of 120 ms and a scanning speed of 0.55 mm/s. The frame rate was set to 8 Hz, the field of view to 90.2 mm, with a spectral binning of 2 and an aperture of 1.9. The data was processed using the ENVI5.4 software, following (Butz et al., 2015). HSI data was calibrated with data obtained from the spectrophotometer measurements for more qualitative estimates of community changes, as calibration and validation with independent data is important (Zander et al., 2022). The procedure is explained in Chapter 4.7.

4.6. Loss On Ignition (LOI) and CNS

Loss on ignition is used to determine the organic matter and carbonate content in lake sediments. Moreover, this method allows the indirect estimation of both organic and inorganic carbon (Heiri et al., 2001; Santisteban et al., 2004). Sediment samples were freeze-dried before they were baked:

1. At 500-550 °C, organic matter is ignited and oxidized to carbon dioxide (CO_2) and ash. The weight loss corresponds to the amount of organic carbon that has ignited from the sample
2. At 900-1000 °C, CO_2 is emitted, leaving calcium oxide (CaO). The weight loss during this reaction corresponds to the amount of CO_2 evolved from carbonate minerals.

Overall, 62 samples were analysed. Before and after each reaction, the sample weight was measured, as the weight loss during the reactions are closely linked to the organic matter and carbonate content (Dean, 1974; Heiri et al., 2001). LOI_{550} and LOI_{950}, representing LOI at 550 °C and 950 °C respectively were then calculated using the following equation (*Equation (7)*, Heiri et al., 2001):

$$LOI_X = \left(\frac{DW_{before} - DW_{after}}{DW_{const}}\right) * 100$$

(7)

Table 3 lists the terms used to calculate LOI_x according to Heiri et al. (2001).

Table 3: *List of terms used to calculate LOI_X, based on (Heiri et al., 2001)*

Term	Definition
LOI_X	LOI at 550 °C (LOI_{550}) or 950 °C (LOI_{950}) as percentage
DW_{before}	Dry weight of the sample before heating [g]
DW_{after}	Dry weight of the sample after heating [g]
DW_{const}	Constant dry weight of the sample before reactions 1 and 2 [g]

The total amount of carbon (TC) is calculated as $1.36 \times LOI_{950}$ (Heiri et al., 2001). Total inorganic carbon (TIC) is $0.273 \times LOI_{950}$ and total organic carbon (TOC) is $TC - TIC$ (Santisteban et al., 2004).

CNS elemental analysis was used to estimate total carbon (TC), total nitrogen (TN) and sulphur (S) content of sediments, Thereby, C, N and S are extracted from the sediment by combusting the samples. C, N and S are then into converted gases, which are separated by using chromatography (Analytical Methods Committee, 2006; Fadeeva et al., 2008). Overall, 62 samples were measured.

The TOC/TN ratio can be used to examine the source of organic matter. As terrestrial plants contain a lot of cellulose and comparably low amounts of proteins, they exhibit high TOC/TN ratios around 20 or even higher. In contrast, phytoplankton show lower ratios (4 to 10). High TOC/TN ratios are thus indicative of organic matter originating from the catchment rather than from aquatic sources (Meyers & Teranes, 2001).

For further analysis two outliers in the LOI obtained water content (at 56 cm and 78 cm) and two outliers in the TOC/TN ratio (at 44 cm and 100 cm) were deleted. The data was then interpolated to fill the gaps. The LOI and CNS data were excluded from the statistical analysis because of their low resolution (2 cm).

4.7. Pigment extraction and spectrophotometric proxy-proxy calibration

Pigment extraction was done according to the SOP at the University of Bern which is based on Lami et al. (2000). Overall, 62 samples were prepared at the University of Bern. For each sample, around 0.5 g of wet sediment was used. 5 ml of acetone 100% HPLC grade were added to each sample to extract the pigments. The samples were then vortexed, sonicated and centrifuged. The separated supernatant was then decanted and stored in a glass vial. Based on the colour of the extracts, the procedure was repeated three to four times until the extracted supernatant was transparent. The samples were then stored at -20 °C. The pigment extractions were then used for both the spectrophotometer and HPLC measurements.

Spectrophotometer measurements were used to investigate the concentration of different pigments and to calibrate the index data obtained from hyperspectral imaging to concentration values. The law of Lambert-Beer (*Equation (8)*) is used to calculate the pigment concentrations based on the absorption spectrum of the sample. The sample is illuminated with light across the spectrum from 900 to 350 nm. For every wavelength, the absorbance of the sample is detected by a sensor (Grasse et al., 2016). We measured 62 samples with the spectrophotometer. To obtain the same spatial resolution for both spectrophotometer and HSI data, HSI data was averaged over every two cm^2. The spectrophotometric measurements were done according to the standard operation protocol (SOP) of the University of Bern, which follows the same procedure as Sanchini & Grosjean (2020).

The pigment extracts were diluted with Acetone (100% HPLC grade) in different ratios to obtain absorption values between 0.2 and 1. The solvent was mixed in micro centrifuge tubes (Tarsons, 1.5 ml) and 400 µl of the mixture was pipetted into a plastic UV-Cuvette with 1 cm of optical path (Brand, 70 µl). The solutions were measured by using a UV-VIS spectrophotometer (Shimadzu, UV-1800 CE, 230 V, 300-900 nm) at 0.1 nm spectral resolution. The wavelength range was set from 900 to 350 nm.

To calculate the concentrations of the pigments in the samples, the obtained absorption spectra was used. The concentrations c (µg/g) of chlorophyll *a* and bacteriochlorophyll *a* were calculated according to the following equation:

$$c = \frac{A_\lambda}{\alpha_\lambda \cdot b} \approx \frac{\frac{A_\lambda}{d \cdot \alpha_\lambda \cdot b} \cdot V_{tot}}{m}$$

(8)

21

which is based on the Lambert-Beer law. b denotes the width of the cuvettes (in this case 1 cm), A_λ (abs) is the maximum absorbance measured at wavelength λ and α_λ (L cm⁻¹ mg⁻¹) is the specific extinction coefficient. The different absorbance coefficients used in this thesis are listed in *Table 5*. d is the dilution factor and is given by the volume of pigment sample divided by the total volume in the cuvette. V_{tot} is the total volume of the pigment extraction (ml). m is the dry weight of the sediment sample (g).

Table 4*: absorbance coefficients (L cm⁻¹ mg⁻¹) for different pigments (Sanchini & Grosjean, 2020)*

Pigments	α_λ (L cm⁻¹ mg⁻¹)	Reference
chloropigments *a*	$\alpha_{666} = 80.77 \times 10^{-3}$	Jeffrey & Humphrey (1975)
bacteriopheophytin *a*	$\alpha_{750} = 52.86 \times 10^{-3}$	Fiedor et al. (2002)

To convert the *RABD* indices to pigment concentrations (µg/g), we built a linear regression calibration curve from the spectrophotometer measurements (*Figure 7*). Both data sets (TChl and Bphe *a*) were standardized and tested for normality (One-sample Kolmogorov-Smirnov and Shapiro-Wilk normality test). To calibrate the data, a standard linear regression model was used (*Equation 9*).

$$y = b_0 + b_1 x$$

(9)

For the statistical analysis, the obtained concentration data was interpolated using a moving average ($k = 0.0687$), followed by averaging the data over every 0.5 cm to match the resolution of the XRF data.

4.8. High Performance Liquid Chromatography (HPLC)

To obtain quantitative measures of more group-specific pigments, high performance liquid chromatography (HPLC) was used. HPLC is a method to separate chemical compounds such as pigments from each other. Based on the affinity of the compounds towards the absorbent material in the static phase, compounds separate from the mixture at different times. The lower the affinity to the static phase, the faster a substance moves through it and separates from the mixture (Sahu et al., 2018). The same pigment extractions used for spectrophotometer measurements were also used for HPLC (Chapter 4.7.). However, only 33 of the 62 samples were measured.

The samples were measured by Dr. Andrea Lami at the Water Research Institute in Verbania by using reversed-phase high performance liquid chromatography. Afterwards, the obtained chromatograms were processed in Chromeleon 7.2. The pigments were assigned based on their absorption spectra and their retention time under the 460 nm and 660 nm channels. The data were used to calculate pigment concentrations in relation to wet bulk weight (*Figure A4*). To do so, standard calibration curves for the different pigments were used to convert the absorbance measures to concentrations in nmol/g wet bulk sediment weight. To obtain the same units [µg/g] as for the spectrophotometer measurements, the concentrations were multiplied by the molecular weight of the according pigments.

Table 5: *List of pigments found in the samples. The affinity, possible use as indicators (proxy) and their stability are given as well. The stability ranges from 1 (high) to 4 (low). Group affiliations are indicated by the different colours: Chlorophylls and derivatives (green), anoxygenic photosynthetic bacteria (purple), Chromophytes (blue), Cyanobacteria (yellow) and Cyanobacteria and green algae (orange). Information in the table are modified from Leavitt & Hodgson (2001), Bianchi & Canuel (2011), Reuss (2005) and in text references.*

Pigments	Affinity	Proxy	Stability
Chlorophylls			
Chlorophyll *a*	Photosynthetic algae, plantae	Total algal biomass	3
Chlorophyll derivatives			
Pheophytin *a*	Chl *a* derivative (senescent diatoms, zooplankton fecal pellets)		1
Pheophorbide *a*	Chl *a* derivative (grazing, senescent diatoms, zooplankton fecal pellets)	Zooplankton grazing, oxidation	3
Bacteriochlorophylls			
Bacteriochlorophyll *a*	chloroflexaceae, chlorobiaceae, purple sulfur bacteria	Anoxygenic phototrophic bacteria (chemocline in meromictic lakes) (Butz et al., 2016)	-
Carotenes			
β-carotene	plantae, algae (chlorophytes, prasinophytes, mesostigmatophytes, rhodophytes), phototrophic bacteria	Primary production, total phosphorus abundance (Leavitt, 1993)	1
α-carotene	cryptophyta, crysophyta, dinophyta, prochlorophytes, rhodophytes, green algae		2
Xanthophylls			
Alloxanthin	cryptophyta, dinophyta, chlorophytes	Water level	1
Astaxanthin	Invertebrate herbivores, N-limited chlorophyta		-
Canthaxanthin	colonial (filamentous) cyanobacteria, invertebrate herbivores	Cyanobacteria (Deshpande et al., 2014)	1
Diadinoxanthin	dinophyta, bacillariophyta, chrysophyta, cryptophyte, diatoms, euglenophyta	Diatoms (Deshpande et al., 2014)	3
Diatoxanthin	bacillariophyta, dinophyta, chrysophyta, diatoms, pyrrophyta	Diatoms (Deshpande et al., 2014)	2
Echinenone	prochlorophytes, cyanobacteria	Cyanobacteria, phosphate eutrophication	1
Fucoxanthin	dinophyta, bacillariophyta, chrysophyta, cryprophyta, algaea of the red algal lineage and brown seaweeds	Diatoms (siliceous algae) (Guilizzoni & Lami, 2003)	2
OH-Spheroidene	*Rhodopseudomonas sphaeroides*		-
Isorenieratene	green sulphur bacteria	*Chlorobium sp.*	1
Lutein	chlorophyta, euglenophyta, plantae	Green algal abundance	1
Okenone	purple sulphur bacteria	*Chromatium sp.*	1
Zeaxanthin	chlorophyta, cyanobacteria, chrysophyta, dinophyta	Cyanobacteria (Deshpande et al., 2014; Guilizzoni & Lami, 2003)	1

4.9. Statistical analysis

After generating the data, we conducted a series of descriptive statistical analyses to obtain a comprehensive overview. Additionally, several multivariate analyses were performed. Prior to statistical analysis, standardization (mean = 0, standard deviation = 1) was applied to both data sets: high-resolution (HSI and XRF) and pigments data. Principal component analysis (PCA) was used to reduce the dimensionality of the data as well as to analyse the compositional assemblage of the sediment core.

To investigate the lithology of the core in the high-resolution data set, unconstrained k-means clustering was used. Subsequently, constrained hierarchical clustering was applied to partition the time series into similar units, i.e. stratigraphic zones. For this purpose, CONISS Constrained Incremental Sum of Squares cluster analysis) method was used (Grimm, 1987). The number of significant clusters was investigated by using the elbow method (Thorndike, 1953), the silhouette method (Rousseeuw, 1987) and the broken stick model (Bennett, 1996). All statistical analyses were conducted using the R statistical software (R Core Team, 2022).

5. Results and interpretation
5.1. Sediment description

Prior to the destructive sediment analysis, an initial visual assessment of the split core was performed. The visual characterisation of the sediment revealed three distinctive units, consistent with the outcomes of unconstrained clustering. *Figure 3* provides an overview of the main sediment features, including results from both LOI and smear slide analysis.

Unit I (115 to 65.5 cm) is characterised by the highest amount of organic matter content (18.9%) and lowest dry bulk density. However, mineral content (58.6%) and calcium carbonate ($CaCO_3$, 22.5%) dominate this lowermost unit. The transition from *Unit I* to *Unit II* is gradual with organic matter content gradually decreasing to 14.5%, while calcium carbonate content gradually increases to 28.1% in *Unit II* (65.5 to 21 cm). The shift from *Unit II* to *Unit III* is more rapid. A further decrease of organic matter can be observed, reaching minimum values of around 12.9%. Calcium carbonates reach their maximum with 30.3 % of the sediment in this uppermost unit.

Unit III (21 to 0 cm) is characterised by bright sediment, featuring around 45 very fine white layers. The presence of very fine laminations in this unit may be explained by the absence of bioturbation under anoxic condition. Anoxic conditions in the hypolimnion favour the preservation of laminations. Permanent lake stratification can lead to oxygen depleted bottom waters. Under these conditions, benthic organisms are limited in their activities or are even unable to persist, leading to reduced sediment disturbance (Zolitschka et al., 2015). Across all three units, minerals dominate the sediment with an overall percentage average of 57.7% over the entire core. The sediment can therefore be classified as clastic (Schnurrenberger et al., 2003).
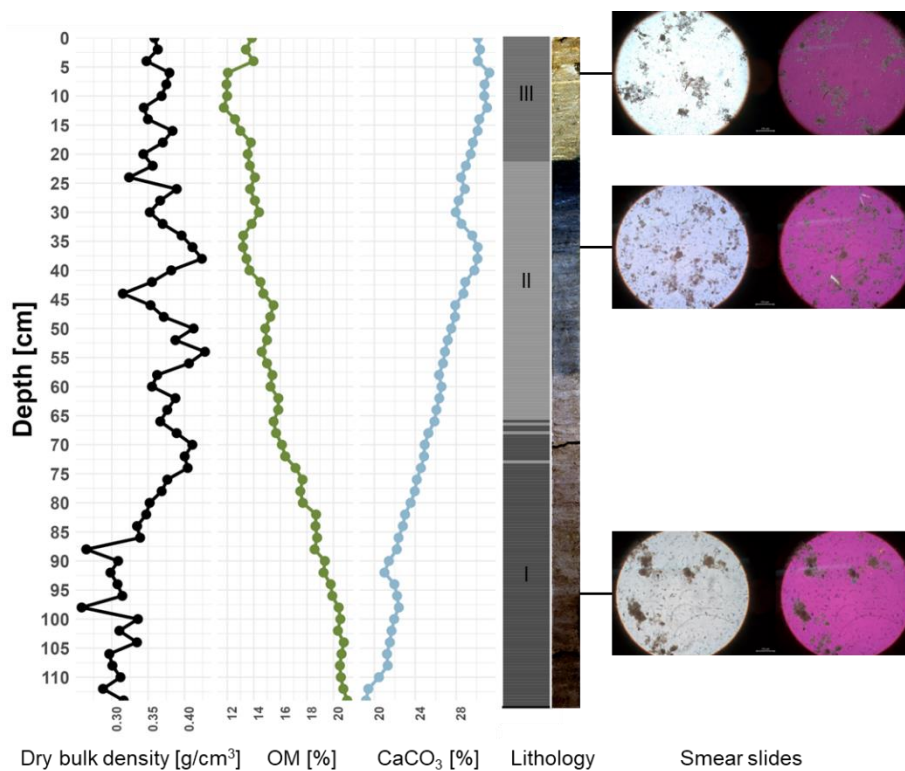
Figure 3: *On the right side, dry bulk density, organic matter content (OM) and calcium carbonate (CaCO₃) from LOI analysis along the depth of the core are plotted. Additionally, a RGB-enhanced core image is shown next to the results from unconstrained clustering on the biogeochemical data. Next to the core image, microscope sediment pictures taken at depths of 2.5 cm, 32.5 cm and 92.5 cm under non- (white) and cross-polarized (pink) light are shown. Smear slides mainly show organic matter content (brown) and carbonates (cross polarized light).*

A summary of the outcomes from the smear slide analysis can be found in *Figure 4*. Compared to LOI, the results depict less pronounced trends in organic matter and calcium particles, appearing rather constant throughout the core. The inorganic matter content mainly persists of carbonates with some silicates and iron oxides. The most distinctive peak in carbonates can be seen at 22.5 cm, followed by a decrease towards the top. Across all three units, carbonates are sharp edged and well defined (mainly subangular in *Units I* and *II* and angular in *Unit III*), suggesting endogenic $CaCO_3$ formation. Warmer temperatures promote enhanced calcium carbonate precipitation due to increased productivity. Increased productivity thereby leads to increased CO_2 consumption. As CO_2, H_2O and $CaCO_3$ are in equilibrium with carbonic acid ($Ca(HCO_3)_2$), the consumption of CO_2 leads to the formation of CO_2, H_2O and $CaCO_3$ from $Ca(HCO_3)_2$. Consequently, $CaCO_3$ is precipitated and sedimented. When CO_2 is abundant, $CaCO_3$ dissolves until it reaches equilibrium with $Ca(HCO_3)_2$ (Cohen, 2003). Endogenic $CaCO_3$ formation is further suggested by the presence of sharp edged and well-defined carbonate particles.

Figure 4 summarizes the main findings from the smear slide analysis. Based on the grain size of carbonate particles, the sediment can be classified as silty clay (finer grains) in *Unit I* transitioning to silt (coarser grains) in *Units II* and *III*. Silicate grains are most common in the deepest 40 cm of the core

but show a strong increase towards the top of the core. Iron oxides are relatively constant, with a slight decrease in the uppermost 32 cm.

Organic matter is predominantly composed of brown amorphous algal material over all three units. Organic matter content within the sediment on the smear slides varies between 46% (82.5 cm) and 59% (52.5 cm) (*Figure 4*).

Planktonic diatoms dominate the diatom counts (*Figure 4*). However, they show a sudden decrease after 22.5 cm, where benthic diatoms become more prominent. The same pattern is reflected in the P:B ratio (planktonic to benthic diatoms). The ratio is highest at 82.5 cm with a ratio of 8 and at 22.5 cm with a ratio of 7.5, where planktonic diatom counts are highest and benthic counts are lowest. The minimum P:B ratio, indicated by a value of 0.86, is observed at a depth of 2.5 cm. The P:B ratio has previously been used to investigate eutrophic conditions based on light penetration into deeper waters (Liu et al., 2020). Under eutrophic conditions, increased aquatic productivity in the epilimnion reduces light penetration into benthic waters, thereby limiting the presence of benthic diatoms (Cohen, 2003). High P:B ratios (P:B > 1) may therefore indicate reduced light availability in benthic waters and productive conditions (Liu et al., 2020). Throughout the sediment core, P:B ratios exceed one, except for the uppermost sample at 2.5 cm. However, interpreting these data may be challenging due to the low overall diatom counts (100). The abundance of chain-forming planktonic diatoms shows an exponential decrease towards the top. The green algae *Phacotus sp.* (Schlegel et al., 1998) first appears at a sediment depth of 62.5 cm and is most prominent in the uppermost sediment parts (12.5 and 2.5 cm with average counts around 9).
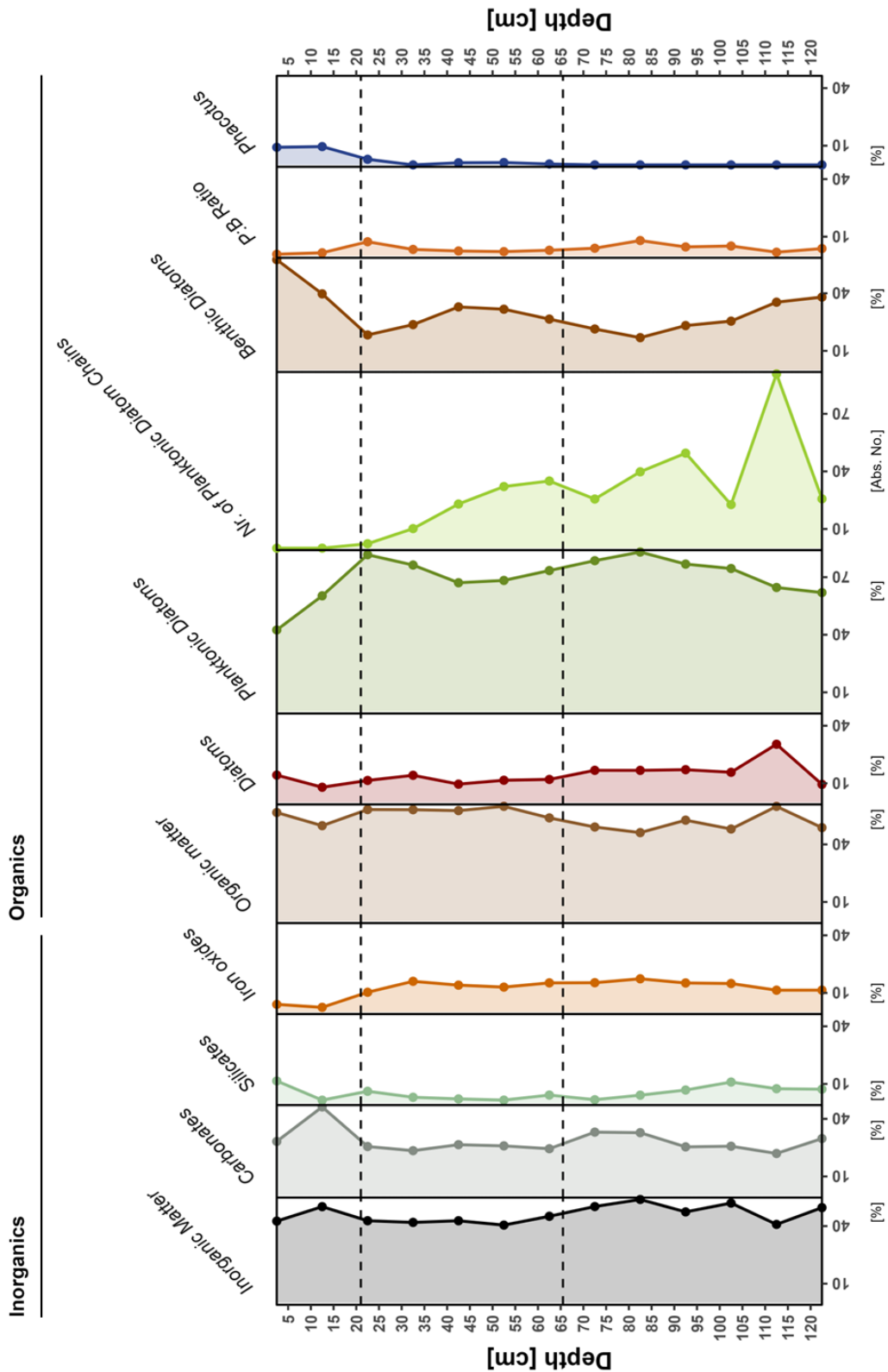
Figure 4: Data obtained from the smear slide analysis given in percentages [%]. Inorganic matter includes total inorganic matter, carbonates, silicates and iron oxides. Organic matter, diatoms and Phacotus sp. make up the total organic matter content. The number of planktonic diatom chains was counted for every slide and given in absolute numbers [Abs. No.]. The P:B ratio is the ratio between planktonic and benthic diatoms. Total inorganic matter and organic matter are given as percentages. All inorganic particles (carbonates, silicates and iron oxides) are then calculated as percentages of total inorganic matter. The same was done for total organic matter.

5.2. Chronology

In *Figure 8*, activity measurements for ^{226}Ra, total ^{210}Pb, unsupported ^{210}Pb and ^{137}Cs are plotted. Both, total and unsupported ^{210}Pb decrease exponentially with sediment depth. The equilibrium line between total ^{210}Pb and ^{226}Ra is reached at 31 cm. The activity of unsupported ^{210}Pb reaches zero at this depth. Up to the sediment depth of 27 cm, ^{137}Cs activity remains below the limit of detection. The first recorded ^{137}Cs activity measurement at 27 cm, therefore, indicates the beginning of nuclear testings in 1954 AD. The ^{137}Cs activity shows two distinctive peaks. The first peak, at 23 cm, is interpreted as the fallout peak in 1963 AD, while the second peak, at 13 cm sediment depth, can be attributed to the Chernobyl accident in 1986 AD. The unsupported ^{210}Pb activity above the limit of detection was used to build a constant rate of supply (CRS) model to establish an age-depth model for AMS22-8. To account for potential losses of unsupported ^{210}Pb activity, the model was corrected by incorporating the missing inventory. The model was further constrained by the 1963 AD ^{137}Cs chronomarker. *Figure 6* provides an overview of the different CRS models. To assess the model fit, chronomarkers from 1954 AD and 1986 AD were incorporated into the figure.

The sediment ages predicted by the model correspond well with those indicated by the peaks in ^{137}Cs activity. The constrained CRS model suggests that the uppermost 29 cm provide insights into approximately the past 71 years, reaching back to 1951 AD. The calculated sedimentation rate (SAR) is relatively constant and varies between 0.388 and 0.471 cm/yr. The mass accumulation rate (MAR) ranges from 0.126 to 0.350 g/cm^{2}yr.
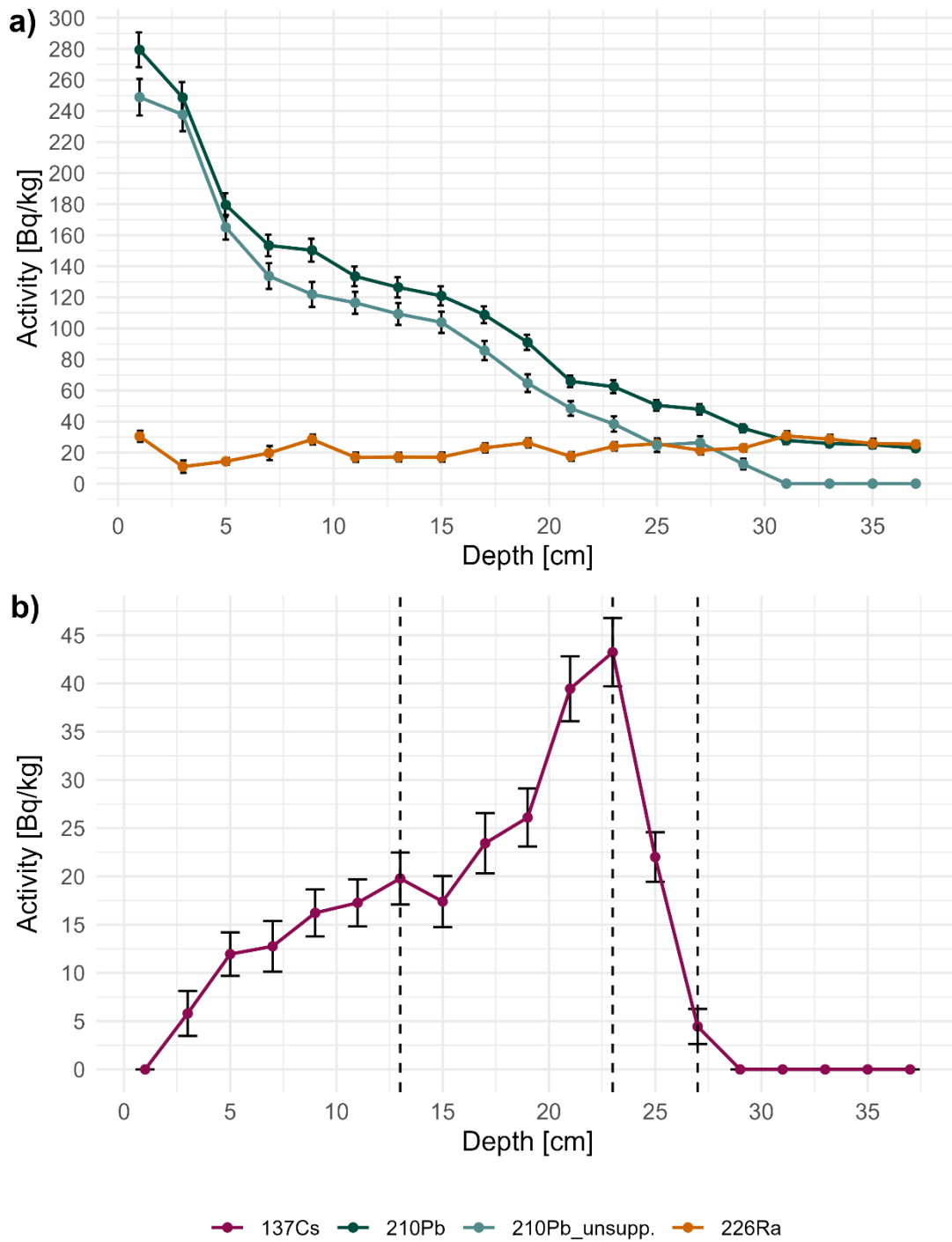
Figure 5: *²¹⁰Pb, ²²⁶Ra and ¹³⁷Cs activity measured by gamma-spectrometry. a) Total ²¹⁰Pb (dark blue), ²²⁶Ra (orange) and unsupported ²¹⁰Pb (light blue) Activity [Bq/kg] plotted against sediment Depth [cm] of AMS22-8. b) ¹³⁷Cs Activity [Bq/kg] (purple) plotted against sediment Depth [cm] of AMS22-8. Chronomarkers derived from 137Cs peaks are indicated as black dashed lines: at 27 cm start of nuclear testing (1954 AD), at 23 cm ¹³⁷Cs peak (1963 AD), and at 13 cm Chernobyl (1986 AD). The samples were taken at 2 cm intervals and were dated using gamma-spectrometry at the University of Gdańsk, Poland by the group of Prof. Dr. Wojciech Tylmann.*
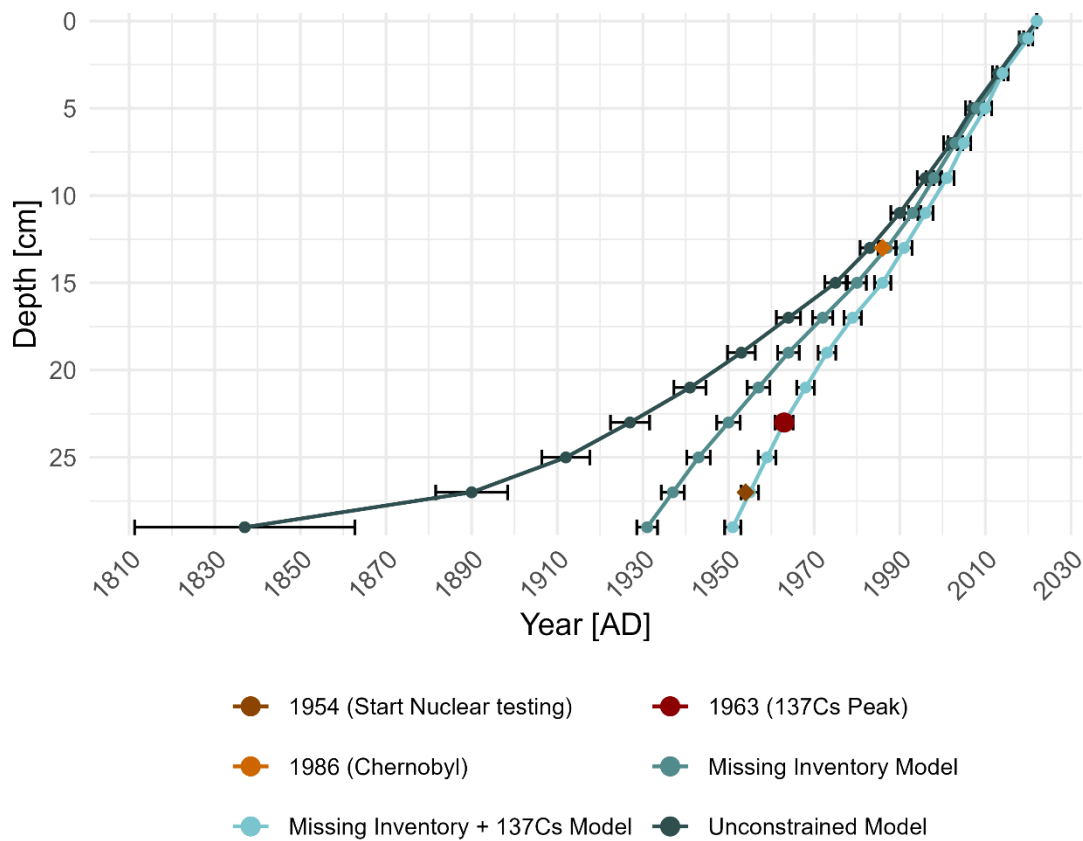
Figure 6: *Results from the Constant Rate of Supply (CRS) model. The blue lines indicate the results from different model runs: Unconstrained Model (dark), Missing Inventory Model (medium) and Missing Inventory + ^{137}Cs Model (light). The dots indicate nuclear events, detected by ^{137}Cs activity in AMS22-8: 1954 AD start of nuclear testing (brown), 1963 AD ^{137}Cs peak (red) and 1986 AD Chernobyl (orange).*

5.3. Spectral indices to concentration calibration

The concentration values of total green pigments and bacteriopheophytin *a* [µg/g] were obtained by calibrating the spectral indices ($RABD_{673}$ and $RABD_{845}$) with spectrophotometric measurements. The calibration lines for both pigment data sets are shown in *Figure 7*. For the calibration, a reduced data set ($n = 11$ for TChl and $n = 10$ for Bphe *a*) was used to ensure normal distribution in the data. The validity of the regression model was checked by running the model with the entire data set ($n = 62$ for both TChl and Bphe *a*).

The reduced total green pigments data set resulted in a Pearson coefficient of $r = 0.84$ with $R^2_{adj.} = 0.67$ ($p = 0.0013$). The root mean squared errors of prediction ($RMSEP$) ranged between 20.98 (k-fold) and 22.59 µg/g (bootstrap) with uncertainties between 26.15 and 28.15%. By using the entire data set for the calibration, the Pearson correlation coefficient could slightly be increased to $r = 0.85$, with the coefficient of determination being $R^2_{adj.} = 0.72$ ($p < 0.001$). Root mean squared errors of prediction ($RMSEP$) differed between 12.13 (k-fold) and 12.43 µg/g (bootstrap) with uncertainties around 15%. Despite the comparable correlation coefficients between the two linear regression models, the $RMSEP$ for the reduced data set is larger. This suggests that, even though the correlation coefficients

are similar, the model using the reduced data set has higher prediction errors than the model using the entire data set. For both data sets, normal distribution of residuals was tested by using the Shapiro-Wilk and the Kolmogorov-Smirnov tests. The results from both tests indicate that the residuals of the two models follow a normal distribution. This confirms that the assumption of normally distributed residuals is met, validating the linear regression models.

For the calibration using the reduced bacteriopheophytin a data set, a Pearson correlation coefficient of $r = 0.93$ with $R^2_{adj.} = 0.85$ ($p < 0.001$) was obtained. $RMSEP$ varied around 1.76 (10-fold and k-fold) to 1.95 µg/g (bootstrap), with the according uncertainties between 15.68 to 17.36% respectively. The Pearson correlation coefficient slightly decreased to $r = 0.91$, with $R^2_{adj.} = 0.82$ ($p < 0.001$), when using the entire data set, $RMSEP$ decreased as well. $RMSEP$ varies between 1.47 (10-fold and k-fold) and 1.51 µg/g (bootstrap). The uncertainties are around 11.6%. While the correlation coefficient slightly decreased, the prediction errors improved by using the entire data set. Again, the Shapiro-Wilk and Kolmogorov-Smirnov tests suggest normal distribution of the residuals for both models. This confirmation of normality allows to draw inferences from the linear regression models.
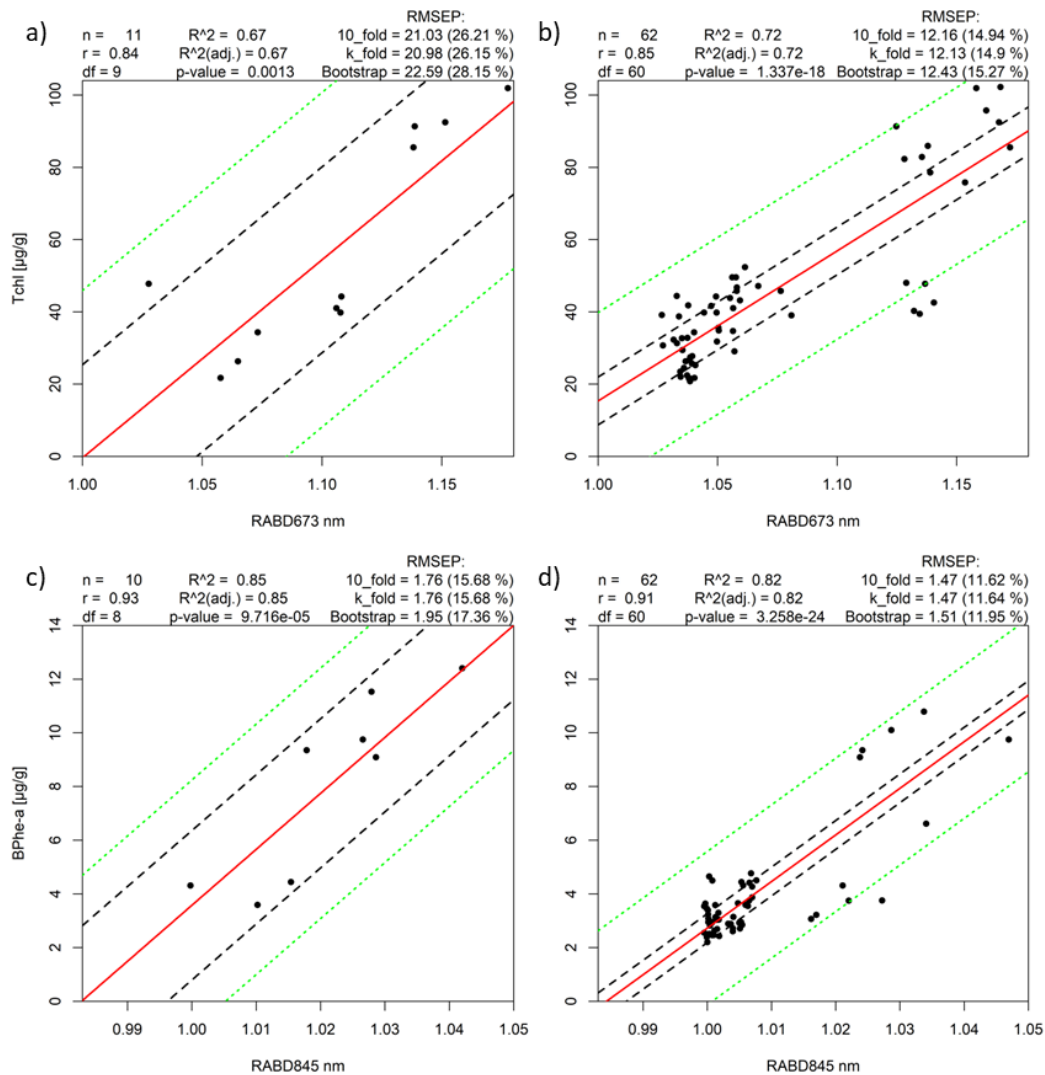
Figure 7: *Spectral indices to concentration calibration models with a) a reduced TChl data set; b) the entire TChl data set; c) a reduced Bphe a data set and d) the entire Bphe a data set. TChl measurements were calibrated with $RABD_{673}$, Bphe a measurements with $RABD_{845}$. The black points indicate the number of samples n. The black dashed line represents the 95% confidence interval for the regression function whereas the green dotted line shows the confidence interval for predicted values.*

5.4. Biogeochemical composition of the sediment

5.4.1. Statistical analysis

The bend in the scree plot of the biogeochemical data (Thorndike, 1953, *Figure 8*) suggests the presence of two main principal components. The first two principal components account for 70.7% of the variance in the data, with PC1 explaining 39.8% and PC2 explaining 30.9%. PC1 is positively associated with elements indicative of erosional input (Si, K, Ti, Mn and Fe) and negatively linked to elements indicative of in-lake formation (Ca, S, Zn, Sr). The strong positive association between PC2 and $RABD_{673}$, $RABD_{710}$ and $RABD_{845}$ implies that the second PC represents aquatic productivity and anoxia.

The biplot of the biogeochemical data is shown in *Figure 9*. $RABD_{620}$, Si, K, Ti, V, Mn, Fe and Rb are mainly associated with *Cluster I*. Al, S, Ca, Ni, Cu, Zn and Sb are mainly linked to *Cluster II* and $RABD_{673}$, $RABD_{845}$, $RABD_{710}$, S and Sr to *Cluster III*. The loadings for the first two PCs are plotted

in *Figure 10*. PC1 is positively linked to $RABD_{620}$, Si, K, Ti, V, Mn, Fe and Rb, whereas $RABD_{673}$, $RABD_{845}$, $RABD_{710}$, Al, S, Ca, Ni, Cu, Zn, Sr and Sb are negatively associated with PC1. $RABD_{673}$ and $RABD_{710}$ have only weak associations with PC1. PC2 is negatively associated with $RABD_{673}$, $RABD_{710}$ and $RABD_{845}$, S, Sr, V and Rb. Conversely, a positive link with PC2 is shown for Si, Ka, Ti, Mn, Fe, Al, Ca, Ni, Cu, Zn and Sb.
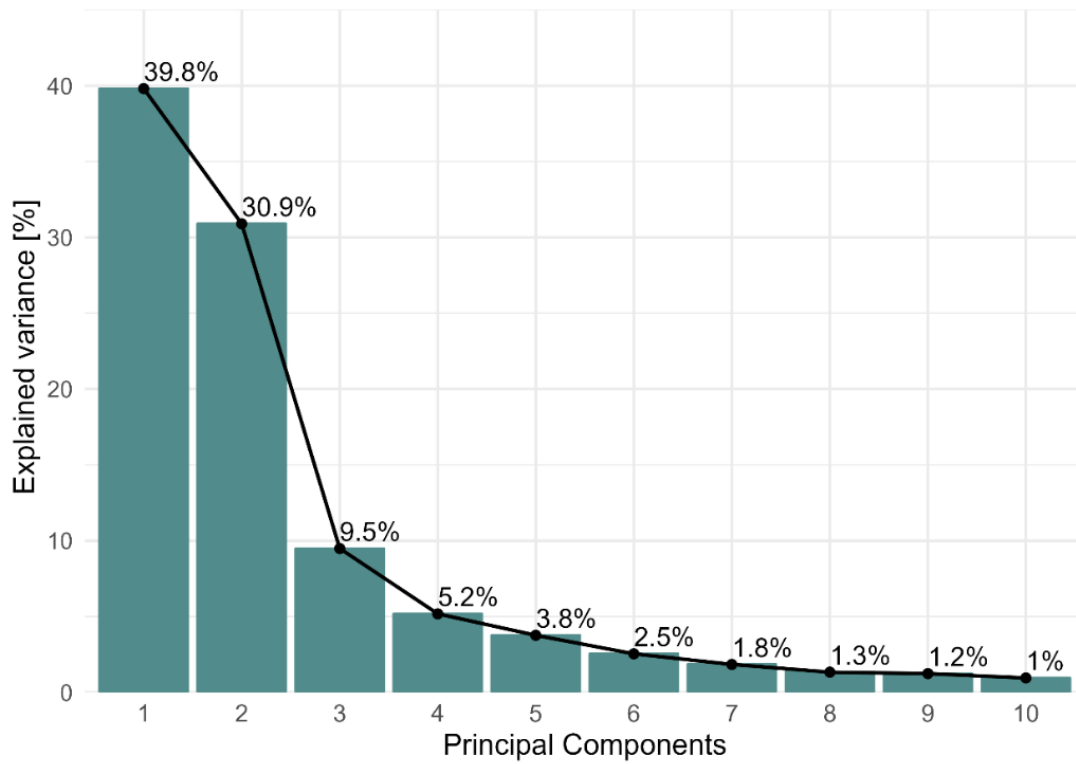

Figure 8: *Scree plot of the biogeochemical data indicating the variance explained by the different principal components (PC).*
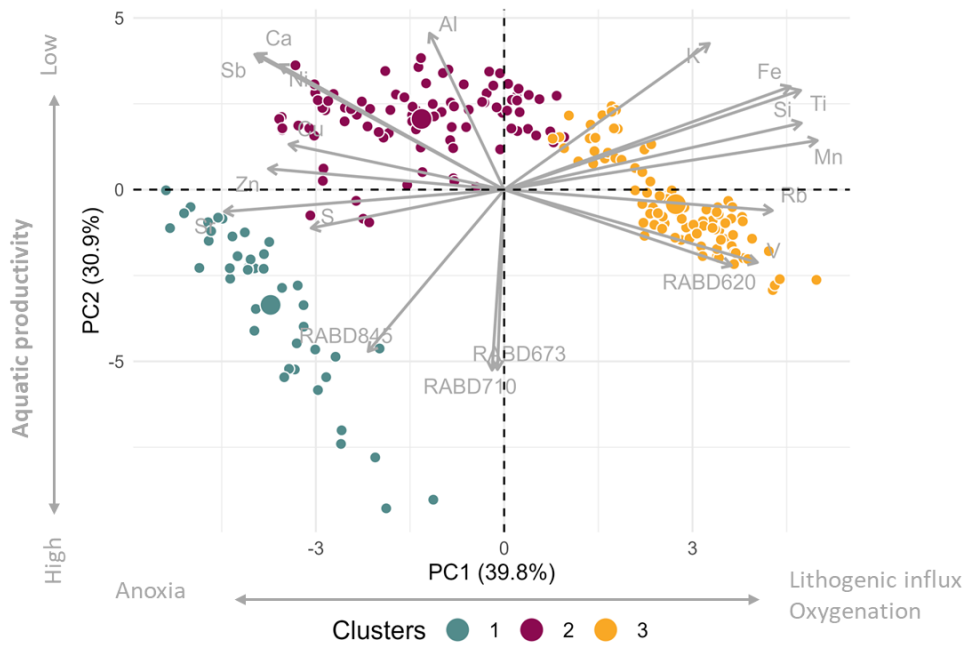
Figure 9: *Biplot of the biogeochemical data with the first two PCs as axes. Each point represents a subsample. The axes indicate the PC scores and the arrows the loading vectors.*
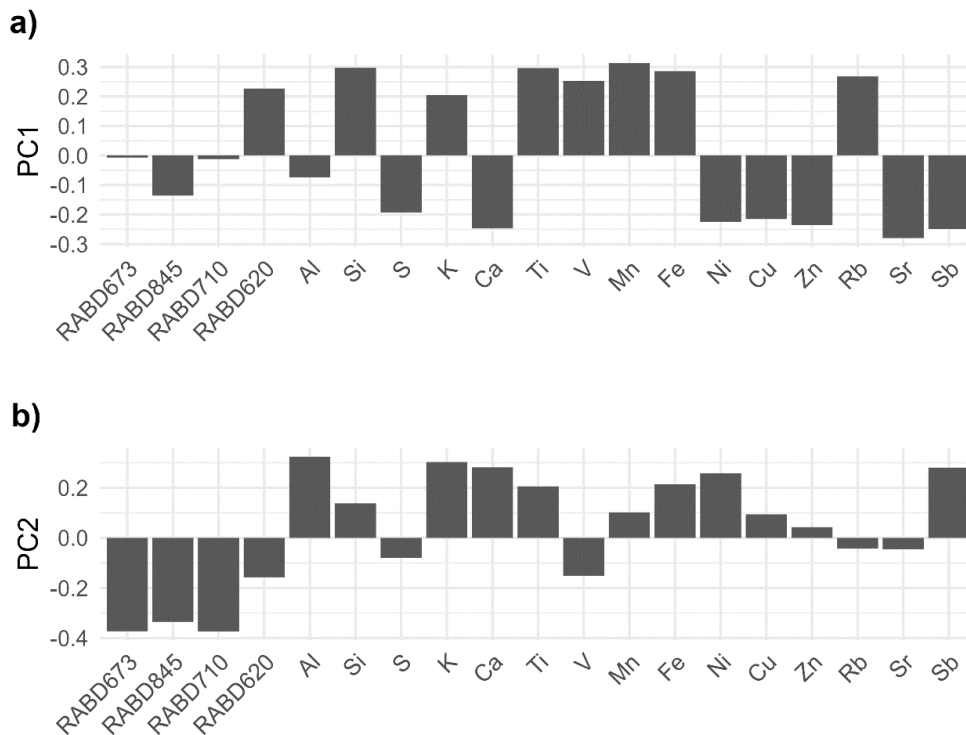

Figure 10: *PC loading of the first two principal components of the biogeochemical data. a) Loadings for PC1. b) Loadings for PC2.*

5.4.2. Biogeochemical stratigraphy

The biogeochemical composition of the sediment core AMS22-8 from Lake Amsoldingen is summarized in *Figure 11*, presented relative to depth. Constrained hierarchical cluster analysis (CONISS-analysis) revealed three distinct biogeochemical zones.

Zone I **(115 to 65.5 cm)**

Intermediate to high total chlorophyll concentrations (TChl) and $RABD_{620}$ values are characteristic for this zone. TChl concentrations and the $RABD_{620}$ indices are used as proxies for aquatic productivity by oxygenic phototrophs (Sorrel et al., 2021; Zander et al., 2022, 2023), indicating high aquatic productivity in this lowermost zone. This is further confirmed by low PC2 scores. Chlorophyll concentrations start to decrease at around 85 cm, whereas cyanobacteria, indicated by $RABD_{620}$, are still abundant, suggesting that cyanobacteria outcompeted other phytoplankton species. Bacteriopheophytin *a* (Bphe *a*) concentrations and $RABD_{710}$ values are low. The reduced Bphe *a* concentrations and the reduced $RABD_{710}$ values suggest at least seasonally oxygenated bottom waters and an absence of permanent lake stratification (Zander et al., 2022, 2023). The high abundance of TChl and $RABD_{620}$ coupled with low Bphe *a* concentrations and $RABD_{710}$ values indicate that the phytoplankton community is predominantly composed of oxygenic phototrophs.

The sediment composition is defined by high counts of titanium (Ti), silicon (Si), iron (Fe) and Manganese (Mn). Mn is only precipitated and sedimented under well oxygenated hypolimnetic waters (Davies et al., 2015; Hamilton-Taylor & Davison, 1995) and, therefore, further supports the lake being in a state with well oxygenated bottom waters. Endogenic calcite precipitation and sedimentation is further shown by increasing Ca counts and its negative association with PC1. An increase in Ti, on the other hand, indicates erosional input from the catchment. Positive PC1 contribution within *Zone I* further represents dominating erosional processes. Comparably high water content can be attributed to higher porosity of the sediment (carbonate silty clay) compared to the upper part of the sediment.

Both, the Inc/Coh ratio and the TOC/TN ratio show comparably low values. The organic matter content in the sediment is primarily linked to aquatic productivity, shown by low TOC/TN values, additionally reflecting high aquatic productivity (Meyers & Teranes, 2001). LOI_{550} is comparably high, while LOI_{950} is low. Sediment water content is fluctuating, but relatively high. PC1 shows a decreasing trend but is overall positive, whereas PC2 increases from negative to slightly positive PC scores.

Zone II **(65.5 to 21 cm)**

Zone II is defined by low pigment concentrations (TChl and Bphe *a*) as well as low *RABD* values, indicating a decrease in aquatic productivity, reaching lowest values. This is shown by TChl, $RABD_{620}$ as well as high PC2 scores. Bphe *a* and $RABD_{710}$ show no sign of lasting bottom water anoxia or permanent lake stratification. The sediment composition changes towards higher counts of Ca and

slightly lower counts of Ti, Si, Fe and Mn, all displaying a slight decreasing trend. Towards the end of *Zone II*, sulphur (S) and zinc (Zn), along with the Fe/Mn ratio, show rising values. This co-occurring increases in Fe, S and Zn suggest in-lake formation and deposition of iron-sulphide minerals such as pyrites and zinc-sulphide minerals such as sphalerites (ZnS, Juillot et al., 2023). A transition from positive to negative PC1 values additionally shows that in-lake processes become more important. The Fe/Mn ratio can be used as an indicator of bottom water oxygenation and reducing conditions, with high values indicating a lowering of bottom water oxygenation and increasing reducing conditions. The rising values towards the top of *Zone II* would, therefore, suggest the onset of anoxic conditions. The Fe/Mn ratio, however, is mainly driven by very high Fe counts (up to 66000 cps) compared to Mn counts (up to 13000 cps) and may, therefore, not be representative for lake water oxygenation.

The Inc/Coh ratio maintains relative stability, whereas the TOC/TN ratio first shows an increase until 36 cm, followed by a slight decrease. Thus, sources of organic matter in the sediment change from aquatic to terrestrial. A decreasing trend can be observed for LOI_{550}, while LOI_{950} increases similar to Ca. Throughout *Zone II*, water content remains comparably low, which can be explained by a change from higher to lower porosity sediment (silty clay to silt) from *Zone I* to *Zone II*.

Zone III (21 to 0 cm)

The transition from *Zone II* to *Zone III* is characterized by a sudden increase in pigment concentrations (TChl and Bphe *a*) and *RABD* values ($RABD_{710}$ and $RABD_{620}$) at a depth of 21 cm. Overall, pigment concentrations and $RABD_{710}$ and $RABD_{620}$ are higher compared to previous zones. An overall negative decreasing trend is observed for PC2 score. PC2 is negatively associated with aquatic productivity ($RABD_{673}$) and anoxia ($RABD_{710}$ and $RABD_{845}$), indicating changes in the lakes' trophic state and mixing regime. The high abundance of TChl, $RABD_{620}$ and Si/Ti and low PC2 scores thereby suggest high aquatic productivity in *Zone III*. High values in Bphe *a* and $RABD_{710}$ indicate co-occurring anoxic conditions and permanent lake stratification. Pigment concentrations and $RABD_{710}$ reach their maximum at around 5 cm sediment depth. This further increase in Bphe *a* and $RABD_{710}$ may thereby represent a community shift from oxygenic phototrophs to anoxygenic phototrophic phytoplankton species. The Si/Ti ratio shows a similar increasing trend as the pigment data but slightly lags behind before decreasing at 7.5 cm. High Si/Ti ratios are often associated with increased biogenic silica production, indicating diatom abundance. A similar decrease can also be observed for ($RABD_{620}$) values. The further increase in TChl towards the top and the decreases in cyanobacteria ($RABD_{620}$) and diatom (Si/Ti) abundance suggest outcompetition of cyanobacteria and diatoms by other phytoplankton species.

Until a depth of 7.5 cm, the sediment is dominated by Ca, before it suddenly decreases. Fe, Mn and the Fe/Mn ratio further decrease towards the top of the core. Decreasing counts in these redox sensitive elements further confirm anoxic bottom water conditions. Redox sensitive elements are dissolved from the sediment under these reducing conditions, leading to a decrease in counts in the sediment (Davies et

al., 2015). The same can also be observed in the decreasing Ca counts towards the top. Under anoxic conditions, the pH decreases, leading to a release of $CaCO_3$ from the sediment to the water column (Shapley et al., 2005). This pattern suggests a transition from well oxygenated hypolimnetic waters to more anoxic conditions. A decrease in both Ti and Si counts, coupled with negative PC1 scores, indicates low erosional input.

The Inc/Coh ratio remains low prior to a sudden increase at 2.5 cm. LOI_{550} decreases further, reaching its minimum in this zone. Increases in Inc/Coh ratio and LOI_{550} from 6 cm onwards show elevated organic matter content in the sediment at the very top of the core. The highest values in the TOC/TN ratio are reached around 6 cm, following a slight decrease. The drop in the TOC/TN ratio indicates high contribution from aquatic sources to the organic matter content of the sediment (Meyers & Teranes, 2001). Higher water content within this zone may be explained by high terrestrial organic matter content.
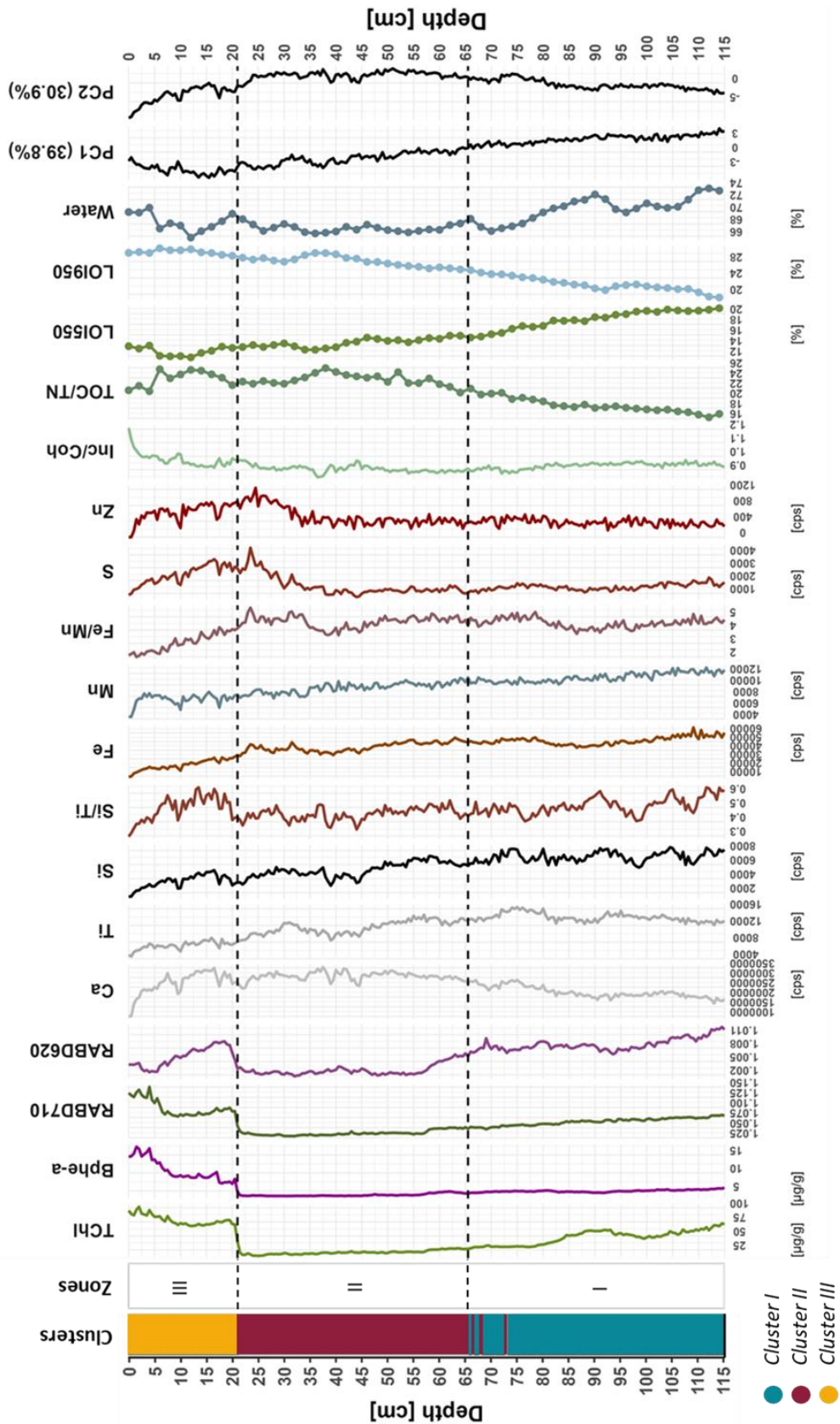
Figure 11: *Selected biogeochemical data of AMS22-8 measured with XRF, HSI, LOI and CNS analysis. Pigment concentrations are given in µg/g, XRF data as absolute counts per second [cps] and low-resolution data as percentages [%]. Additionally, PC1 and PC2 scores are plotted. On the left side, the results obtained from unconstrained k-means clustering (Clusters) are shown, indicating the lithology of the sediment. The zones (CONISS-analysis) are shown next to the unconstrained clusters and indicated as black dotted lines.*

38

5.5. Pigment composition
5.5.1. Statistical analysis

Principal component analysis on the pigment data revealed that 82.8% of the variance is explained by the first two principal components (*Figure 12*). PC1 thereby explains 67.9% of the variance. Except for diatoxanthin, the chlorophyll preservation index (CPI) and the CD/TC ratio, all variables are negatively correlated with PC1 (*Figure 13*). Diatoxanthin, CPI and CD/TC are primarily linked to *Cluster I (Figure 14)*. The pigments negatively linked to PC1 are mainly associated with *Cluster III*, dominated by pigments of cyanobacteria and anoxygenic photosynthetic bacteria. PC2 explains 14.9% of the variance in pigment assemblage. Chlorophylls and derivatives, fucoxanthin, diatoxanthin, astaxanthin, CPI and CD/TC show clear positive associations with PC2. The loadings of the remaining pigments do not show clear positive or negative loadings for PC2.

The strong negative association between PC1 and almost all pigment variables suggests that PC1 is representative for aquatic productivity. The pattern for PC2 is less clear. Its strong positive association with TChl, Chl *a*, fucoxanthin and diatoxanthin, all linked to relatively low stability (Leavitt & Hodgson, 2001), suggests a link to high diatom abundance. On the other hand, pheophorbide *a* (Leavitt & Hodgson, 2001), astaxanthin (Makri et al., 2019), the CPI (Buchaca & Catalan, 2008) and CD/TC (Swain, 1985) are all related to pigment preservation or zooplankton grazing. However, considering that both CPI and CD/TC are derived from chloropigment concentrations and do not provide independent measures of zooplankton grazing, we propose that positive associations with PC2 are primarily linked to diatoms. APB, chromophytes which are not associated with diatoms, cyanobacteria and green algae show a slight negative association with PC2.
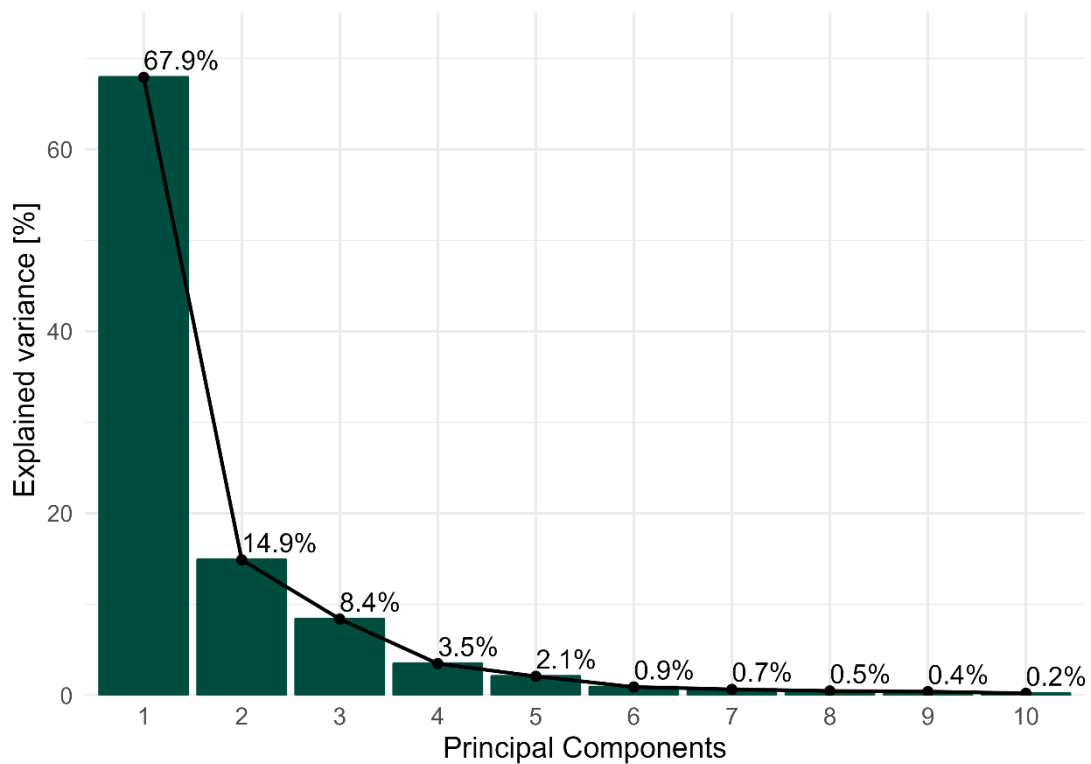
Figure 12: *Scree plot of the pigment data indicating the variance explained by the different principal components (PC).*
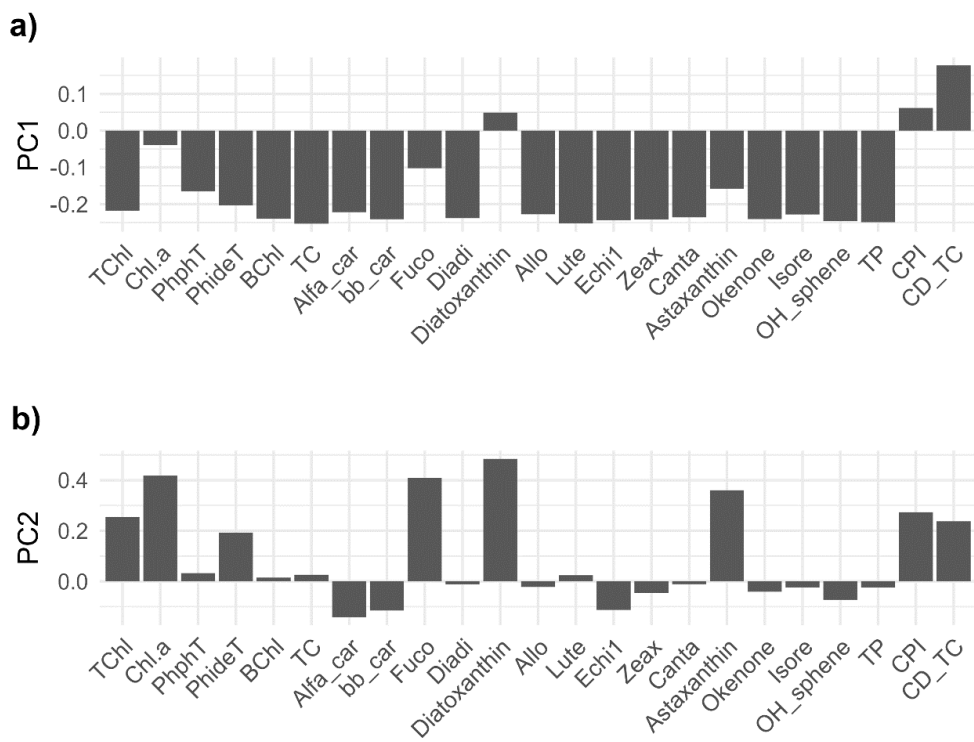

Figure 13: *PC loading of the first two principal components of the pigment data. a) Loadings for PC1. b) Loadings for PC2.*
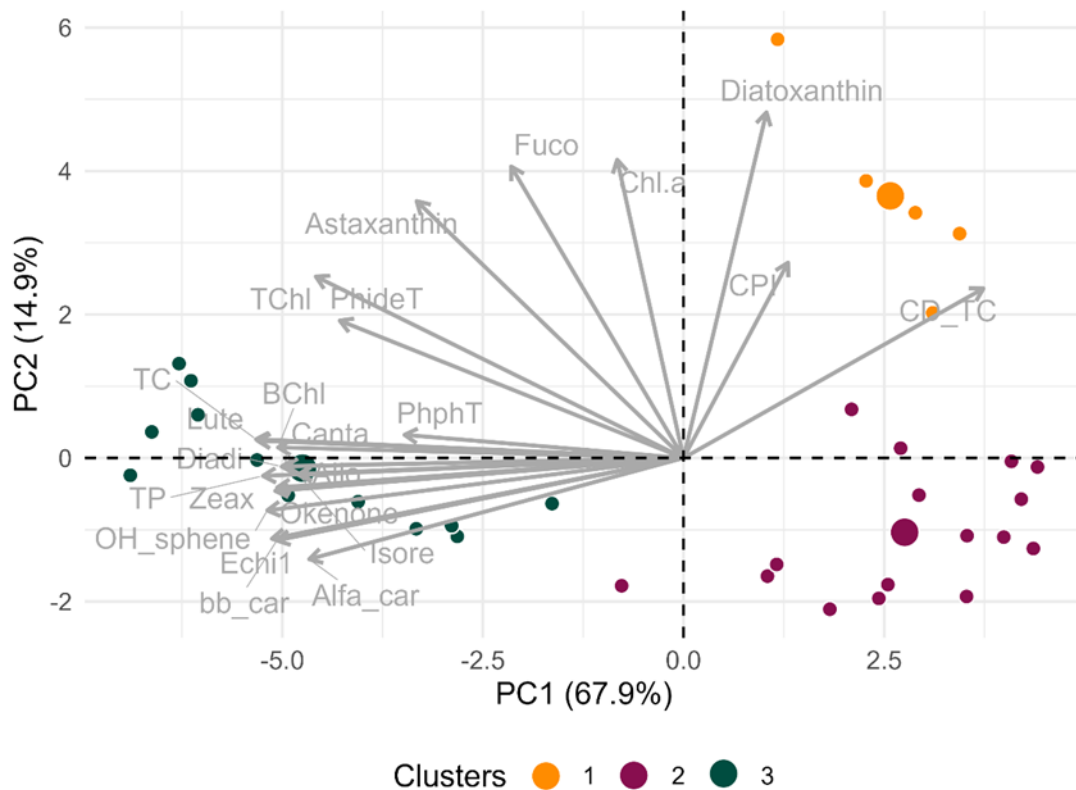
Figure 14: *Biplot of the pigment data with the first two PCs axes. Each point represents a certain subsample. The axes indicate the PC scores and the arrows the loading vectors.*

5.5.2. Pigment stratigraphy

The pigment stratigraphy of Lake Amsoldingen is summarized in *Figure 15*. The constrained hierarchical cluster analysis (CONISS-analysis) resulted in three distinctive pigment zones, slightly different than the biogeochemical zones (*Figure 11*).

Pigment Zone I (125 to 82 cm)

Elevated concentrations of total chlorophylls obtained from HSI (TChl cal.) as well as from HPLC (TChl) measurements and total chlorophyll-*a* concentrations and their derivatives (pheophytin *a* and pheophorbide *a*) in *Pigment Zone I* suggest productive conditions. The abundance of pigments associated with chromophytes like fucoxanthin, diatoxanthin and astaxanthin further supports this indication. Fucoxanthin and diatoxanthin serve as indicators for diatoms (Deshpande et al., 2014; Guilizzoni & Lami, 2003). Diatoms are often associated with low nutrient conditions as they are good competitors for phosphorus (Wetzel, 2001). High CD/TC values can further be interpreted as a trophic state change towards lower nutrient (non-eutrophic) conditions (Guilizzoni & Lami, 2003). Mesotrophic conditions are suggested by low TC-inferred TP concentrations. Phosphorus in the water column is bioavailable and constantly used. Consequently, increased productivity coupled with low TC-inferred TP concentrations may indicate that phosphorus is the limiting factor for aquatic productivity (Correll, 1999).

Indicators of APB are sparce as suggested by low concentrations of HIS-derived bacteriopheophytin *a* (Bphe *a* cal.), HPLC-derived bacteriochlorophyll *a* (BChl *a*), okenone, isorenieratene and OH-spheriodene. High epilimnetic productivity reduces the amount of light reaching the chemocline and thereby limits the growth of PSB (Bphe *a*, BChl *a* and okenone) (Zander et al., 2023). Frequent mixing and subsequent oxygenation of bottom waters further reduce the presence of APB (Zander et al., 2023). However, the detectable presence of pigments produced by APB suggests at least seasonally anoxic bottom water conditions (Zander et al., 2021). The conditions within this zone can thereby be described as highly productive with a holomictic mixing regime. Even though our data suggests at least seasonally oxygenated bottom water, pigment preservation is not affected as shown by high CPI values. Overall high CPI values as well as a slight peak in BChl *a* concentrations may indicate good pigment preservation under seasonally anoxic conditions (Reuss et al., 2005). High CD/TC ratio values, however, indicate low pigment preservation (Swain, 1985). Elevated values of pheophorbide *a* and astaxanthin suggest zooplankton grazing (Leavitt & Hodgson; 2001, Makri et al., 2019) within this pigment zone. Overall, high aquatic productivity in *Pigment Zone I* is driven by oxygenic photosynthetic bacteria, mainly associated with diatoms and potentially other chromophytes (bacillariophyta, chrysophyta, cryprophyta and dinophyta).

Pigment Zone II (82 to 20 cm)

The overall low pigment concentrations within this pigment zone suggest that aquatic productivity was not particularly high. The remaining low levels of APB suggest regular lake mixing and bottom water oxygenation. High CD/TC values and low TC-inferred TP concentration further point towards mesotrophic conditions. HPLC pigment measurements peak at 30 cm sediment depth. After this peak, HPLC derived pigment concentrations slightly decrease before rising towards the end of the zone. Pigment concentrations obtained from HSI calibrations exhibit a slight lag in this increase, with a very sudden increase in TChl and Bphe *a* concentrations at 21 cm. The uppermost part of *Pigment Zone II* can, therefore, be interpreted as the onset of modern eutrophication and anoxia.

Pigment Zone III (20 to 0 cm)

This pigment zone is defined by high pigment concentrations, indicating the establishment of modern eutrophication. The establishment of modern eutrophication is not only reflected in high pigment concentrations but also in comparably low CD/TC ratios. Low CD/TC ratios, however, can also be indicative for high abundances of cyanobacteria or even cyanobacteria dominance of the phytoplankton community (Guilizzoni & Lami, 2003; Swain, 1985). *Pigment Zone III* is mainly associated with negative PC2 scores, indicating cyanobacteria, green algae, APB and chromophyte (others than diatoms) abundance. Compared to previous pigment zones, cyanobacteria abundance (zeaxanthin, canthaxanthin and echinenone) drastically increased in this uppermost pigment zone. However, the rest of the pigments are high as well. Thus, the low CD/TC ratios in this pigment zone are interpreted as indicators of eutrophic conditions and high abundance of cyanobacteria rather than cyanobacteria dominance. Unlike

the rest of the pigment measurements, the rise in Chl *a* concentration is not as pronounced. Pheophorbide *a*, a stable degradation product of labile Chl *a*, can be produced during zooplankton grazing of Chl *a* (Reuss et al., 2005b). The high concentrations of pheopigments (pheophytin *a* and pheophorbide *a*) as well as low CPI values suggest poor Chl *a* preservation, potentially explaining the comparably low Chl *a* concentrations (Zander et al., 2021). Therefore, the TChl contrarotations obtained from HPLC measurements are mainly influenced by degradational products, contributing to the discrepancies between TChl and Chl *a* concentration. Consistently high pigment concentrations are also observed for chromophytes as indicated by fucoxanthin, diadinoxanthin, alloxanthin, astaxanthin and α-carotene, pigments associated with cyanobacteria (echinenone, canthaxanthin, β-carotene, lutein and zeaxanthin) and with green algae (β-carotene, lutein and zeaxanthin), indicating phytoplankton blooms. Elevated concentrations of the cyanobacteria pigment echinenone are further associated with phosphate eutrophication (Guilizzoni & Lami, 2003).

The abundance of OH-spheroidene rather than spheroidene is associated with temporary oxygen availability in small amounts within hypolimnetic waters (Züllig, 1986). Conversely, an increase in isorenieratene concentrations, representing elevated GSB concentrations, is often interpreted as a sign of permanently anoxic conditions (Zander et al., 2023). However, concentrations of pigments indicative of GSB are considerably higher than those of OH-spheroidene and reach their maximum at 4 cm when OH-spheroidene already slightly decreases. The same trend is shown by PSB pigments (Bphe *a* cal., BChl *a* and okenone). TC-inferred TP concentrations reach their maximum. The anoxic conditions in the hypolimnetic waters may lead to P release from the sediment to the water column (Tu et al., 2020), making it available for bioproductivity. However, due to the permanent lake stratification, P cannot be brought up to the epilimnion and thus accumulates in the water (Cohen, 2003). The shift from holomictic to meromictic conditions in this uppermost pigment zone resulted in a change in phytoplankton community composition, shown by a transition from oxygenic phototrophs (cyanobacteria, green algae and chromophytes) to APB.
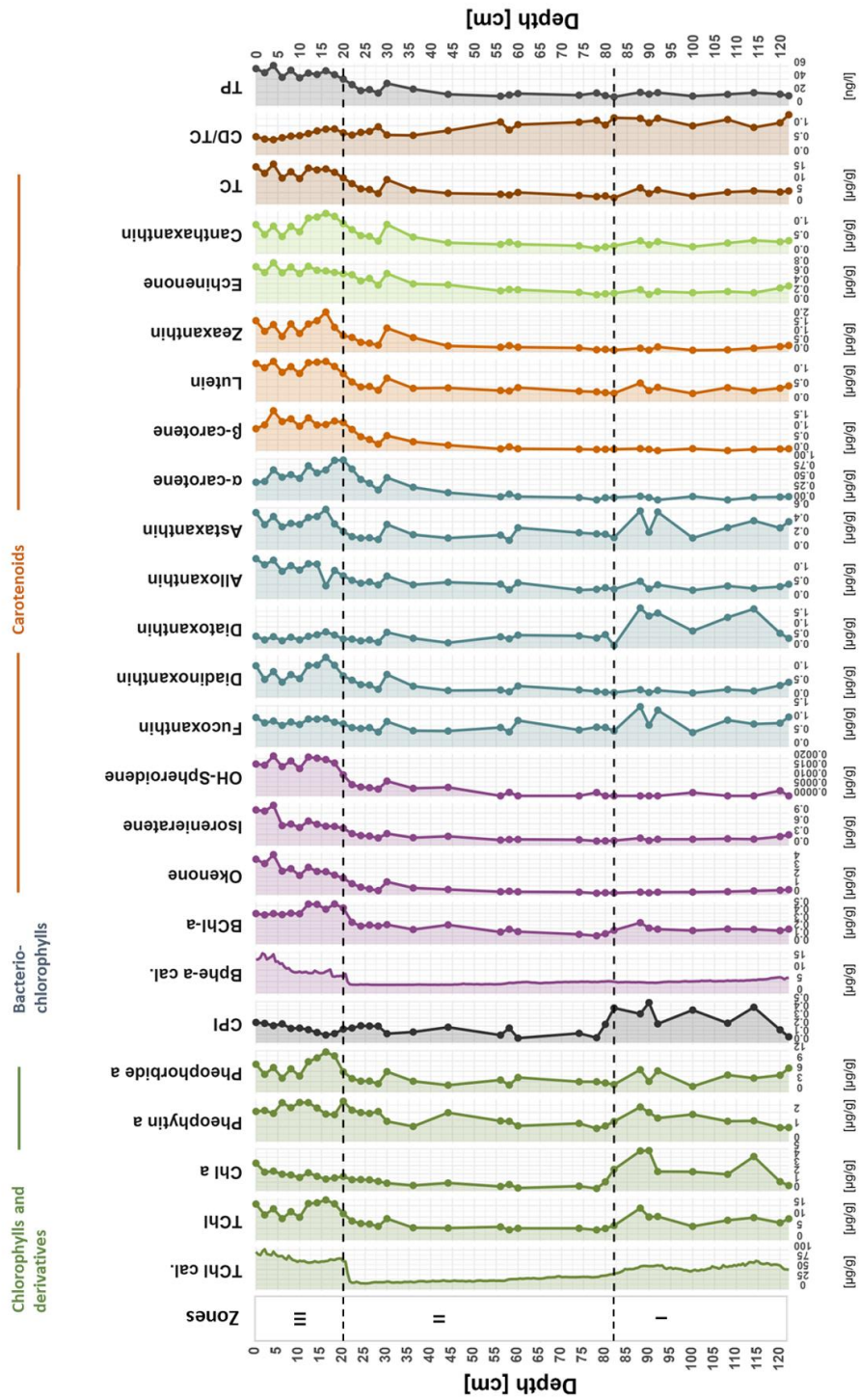
Figure 15: *Pigment stratigraphy representing HSI-inferred pigment concentrations as well as measurements obtained from HPLC analysis. All pigment concentrations are given in µg/g. Total phosphorus concentrations (TP) are given in ng/l. The pigment zones obtained from constrained hierarchical clustering are indicated by the black dotted lines. Blue lines are indicative of pigments associated with chomophytes, light-green with cyanobacteria and orange ones with cyanobacteria and green algae.*

6. Discussion

6.1. The last millennium

By using ^{210}Pb dating, we date the uppermost 29 cm of sediment back to the year 1951. Throughout this period, SAR remained relatively constant, ranging from 0.388 to 0.471 cm/yr. The Ti profile indicates that erosional input was highest in the lowermost zone of the sediment, gradually decreasing towards the top of the core. This is further supported by the positive loadings of PC1 in *Zone I*, representing erosional input in *Zone I*. This further supports our assumption that SAR was highest in *Zone I*, driven by high erosional input and aquatic productivity (chloropigment and chromophyte concentrations, $RABD_{720}$ index) from 125 to 82 cm. A sudden increase in SAR, attributed to rising erosional input and aquatic productivity, is commonly linked to anthropogenic landscape clearance, as documented by Zander et al. (2021). The gradual deforestation of the catchment of Lake Amsoldingen over the past 2000 years (Lotter & Boucherle, 1984) aligns with this trend, potentially contributing to the expected rise in SAR over this period. Further considering productivity and anoxia data from other Swiss Plateau lakes, we hypothesize that AMS22-8 covers approximately one thousand years.

The past millennium can be divided into three main stages: the Medieval Climate Anomaly (MCA), the Little Ice Age (LIA) and the 20th century. The MCA represents a preindustrial warm period (Wanner et al., 2022). Makri et al. (2020) reported enhanced aquatic productivity and reduced anoxic conditions during the MCA in Moossee, a Swiss Plateau lake. The latter was also reported for Soppensee (Tu et al., 2021). High aquatic productivity and Ti counts as well as low APB concentrations are shown in the lowermost approximately 40 cm of AMS22-8, suggesting that this period might correspond to the MCA. During LIA, a cold period lasting from 1250 to 1860 AD (Wanner et al., 2022), Moossee experienced a decline in aquatic productivity (Makri et al., 2020). A sudden decrease in pigment concentrations around 82 cm sediment depth in Lake Amsoldingen aligns with this trend, indicating a potential response to the decreasing temperatures during LIA. Subsequently, aquatic productivity in Moossee recovered around 1850 AD before reaching maximum values in the twentieth century (Makri et al., 2020). A similar shift from low to high aquatic productivity is evident in Lake Amsoldingen, with an unprecedented increase in the 1950s AD.

To analyse our results in the context of the proposed time period covered by AMS22-8, *Figure 16* provides an overview of selected productivity (TChl cal., TChl) and anoxia (Bphe *a* cal., BChl *a*) data, as well as European precipitation (Amann et al., 2015) and summer temperature reconstructions (Luterbacher et al., 2004, 2016). The data was visually fitted under the assumption that our data reaches back approximately one thousand years. The expected ending of the MCA, marked by a sudden decrease in pigment concentrations at 86 cm, served as a reference point for visual alignment. The uppermost 29 cm were matched based on sediment ages. In the following, the data is discussed within the different pigment zones obtained from hierarchical clustering on the pigment data set.
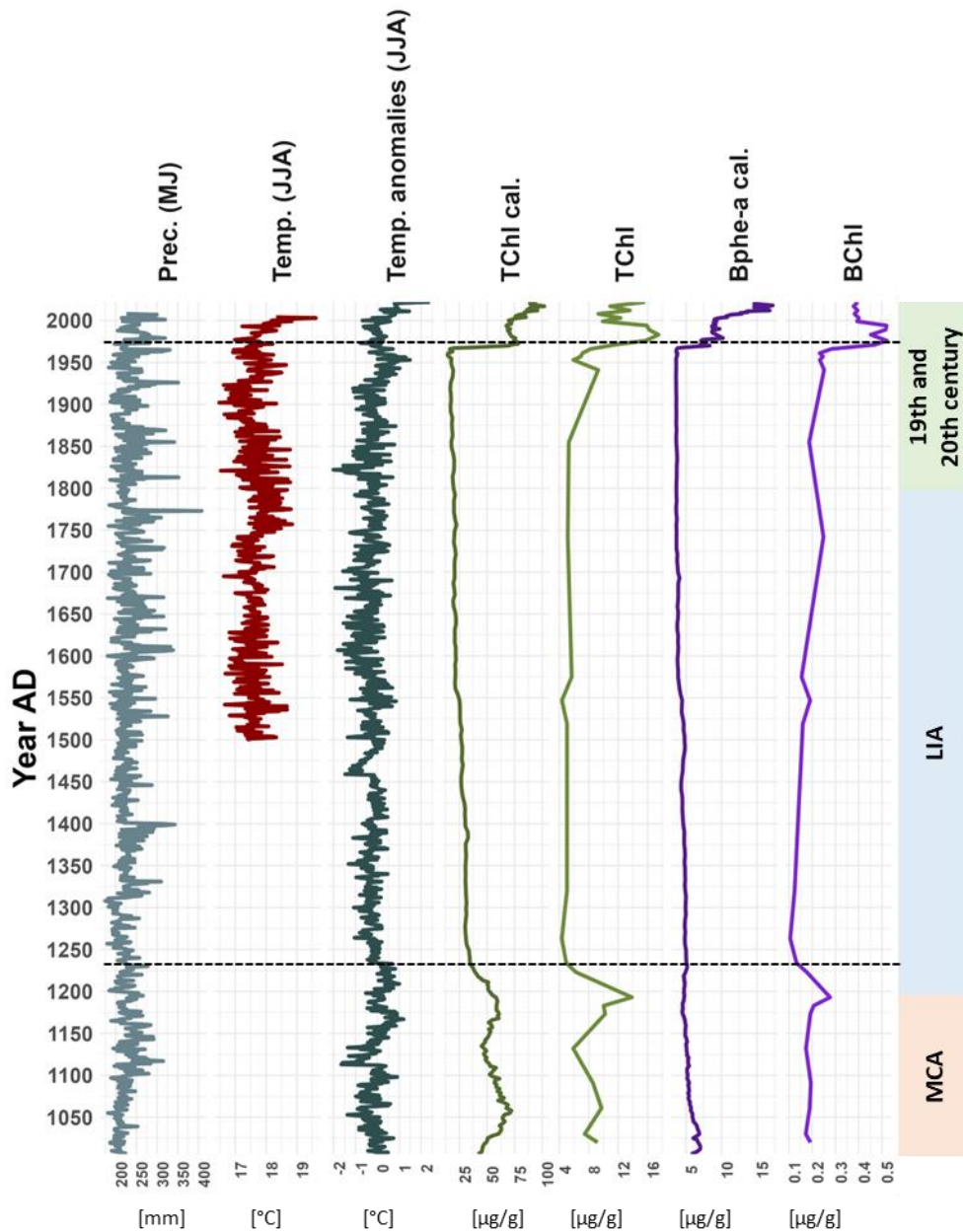
Figure 16: *Summary of lake productivity (TChl cal., TChl) and anoxia (Bphe a cal., BChl) plotted alongside Central European (north of the Alps) May-June precipitation (Amann et al., 2015) and summer (June, July, August) temperature reconstructions (Luterbacher et al., 2004, 2016). Temperature anomalies (Luterbacher et al., 2016). The climate data is visually aligned with the productivity and anoxia data and should be interpreted as an estimated fit. From 1951 AD upwards, the data has been fitted based on actual sediment ages. Black dotted lines indicate the pigment zones derived from hierarchical clustering on the pigment data set. On the right side, the different climatic periods are indicated: MCA, LIA and the last two centuries.*

6.2. Reconstructing aquatic productivity and anoxia in Lake Amsoldingen

Hyperspectral imaging enables us to compile high-resolution pigment data. Calibrating the data with spectrophotometer measurements results in high resolution pigment concentrations and thus more quantitative estimates of pigment dynamics. The resulting high resolution data can even capture short-term changes in trophic states and oxygenation levels (Zander et al., 2022). Combining the high-resolution pigment data with HPLC measurements for pigment identification and quantification, along with XRF measurements, enabled us to investigate paleolimnological conditions and phytoplankton

community changes in Lake Amsoldingen. Although Lake Amsoldingen has been previously studied by Lotter & Boucherle (1984), the last millennium was not their subject of interest. Despite sporadic measurement records related to the lake's trophic state, little is known about aquatic productivity and anoxia in Lake Amsoldingen. In this study, we were able to show how aquatic productivity and anoxia changed over the last approximately one thousand years at this site.

6.2.1. Aquatic productivity and trophic state of Lake Amsoldingen

Pigment Zone I: **High aquatic productivity prior to increased eutrophication**

The hyperspectral imaging data align well with HPLC derived pigment concentrations. For both methods, *Pigment Zone I* is characterized by high aquatic productivity, as indicated by high values of TChl cal., TChl, Chl *a*, pheophytin *a*, pheophorbide *a*, $RABD_{620}$, fucoxanthin, diatoxanthin and astaxanthin. Comparably low TOC/TN but high values within this zone suggest that the sediment's organic matter content is influenced by terrestrial input (Meyers & Teranes, 2001).

The productivity of a lake is influenced by factors such as temperature, nutrient levels, oxygen and light availability (Cohen, 2003; J. Smol et al., 2001; Zander et al., 2021). Considering our assumption that this lowermost cluster corresponds to the MCA, enhanced primary productivity could be attributed to warmer temperatures as found in other studies (Lotter & Boucherle, 1984; Sanchini et al., 2020; Zander et al., 2021). The productivity data plotted in *Figure 16* follows the summer temperature variability nicely, with higher temperature anomalies generally corresponding to higher productivity. However, for many Swiss Plateau lakes (Lobsigensee, Soppensee, Moossee), this period was further characterized by human settlements and intensive deforestation (Guthruf et al., 1999; Lotter, 2001; Makri et al., 2020; Tu et al., 2020). Human settlements and deforestation thereby lead to increased erosional inputs and higher nutrient fluxes into the lake, consequently enhancing aquatic productivity (Lotter, 2001; Makri et al., 2020). 2000 years ago, human settlements and related deforestation first reached the catchment of Lake Amsoldingen (Lotter & Boucherle, 1984). Together with high Ti counts and a positive PC1 score (biogeochemical data), these findings suggest high erosional input due to reduced forest cover. Therefore, we propose that the increased aquatic productivity in *Pigment Zone I* is primarily driven by a combination of climate and early anthropogenic impacts, such as deforestation.

Pigment Zone II: **The transition from low aquatic productivity to highly productive conditions**

Both, HSI and HPLC derived pigment measures indicate low aquatic productivity in the lower part of *Pigment Zone II*. Reports of decreased aquatic productivity during the LIA in other Swiss Plateau lakes, such as Moossee (Makri et al., 2020) and Soppensee (Tu et al., 2021), align with our findings. Lower productivity during LIA is likely explained by lower temperatures associated with the cold phase (*Figure 16*). Around 1950 AD, an increase in productivity (TChl, Chl *a*, pheophytin *a*, pheophorbide *a*, diadinoxanthin, α-carotene, β-carotene, lutein, zeaxanthin, echinenone and canthaxanthin) can be observed. Since the 1950s AD, agriculture in Switzerland has become more intensive, exerting increased

pressure on the environment (BAFU & BLW, 2008). Enhanced aquatic productivity during the mid-20th century as a response to these land-use intensification has also been reported for other Swiss Plateau lakes (Makri et al., 2019, 2020; Tu et al., 2020, 2021) and small Polish lakes (Sanchini et al., 2020; Zander et al., 2021). The change in aquatic productivity within this zone may therefore be attributed to a transition from temperature driven patterns to primarily agricultural influences towards the end of this zone.

***Pigment Zone III* (1968 to 2022 AD): The time of modern eutrophication**

The transition from *Pigment Zone II* to *Pigment Zone III* is marked by a sudden and strong increase in almost all pigment concentrations, indicating enhanced aquatic productivity. Increased aquatic productivity is not only evident in enhanced pigment concentrations but also in a substantial rise in the Si/Ti ratio, indicative of increased diatom abundance. Dated back to the year 1968, this unprecedented increase is likely attributed to modern eutrophication, driven by increased nutrient inputs, a phenomenon reported in other Swiss Plateau lakes (Makri et al., 2019, 2020; Tu et al., 2021). The temperature data in *Figure 16* further suggest that increased productivity is likely attributed to enhanced nutrient inputs into the lake rather than to increased temperatures. While the increase in aquatic productivity in Lake Amsoldingen is sudden, it is not as pronounced as observed in other lakes such as Soppensee (Tu et al., 2021) and Moossee (Makri et al., 2020). During the Second World War, several Swiss Plateau lakes, including Lake Burgäschi, Lobsigensee, Inkwilersee and Moossee, underwent artificial lowering of lake levels and drainage of bog landscapes to expand agricultural fields. This led to the exposure of organic soils to oxygen, leading to the mineralization of organic substances, releasing additional nutrients, such as P and N, into the environment. The overall intensification of agriculture in these areas further contributed to increased productivity (Guthruf et al., 1999). A lowering of the lake level in Lake Amsoldingen was prevented. Additional protection measures, such as protection of the bog landscape and prevention of intensive agricultural practices in nearby parcels, were implemented by previous lake owners (Guthruf et al., 1999). These measures may have played an important role in mitigating the lake's response to increased human impacts, such as intensified agriculture, and could explain the weakened reaction compared to other lakes. Nowadays, extensive agriculture, mainly grassland, continuous to dominate the catchment of Lake Amsoldingen.

6.2.2. Anoxia, mixing regimes and stratification in Lake Amsoldingen

***Pigment Zone I:* Wind-induced mixing as a response to deforestation**

The generally low presence of Bphe *a* cal., BChl *a*, okenone, $RABD_{710}$, isorenieratene and OH-spheroidene imply seasonal lake stratification and anoxic bottom waters during summer. Anoxic conditions are tightly linked to temperature changes. During warm periods, such as the MCA (*Figure 16*), bottom water anoxia may establish as a response to enhanced lake stratification, similar to what occurred in Lake Amsoldingen during the Bølling (Guthruf et al., 1999; Lotter & Boucherle, 1984). Thereby, the oxygen transportation from the epilimnion to the hypolimnion is inhibited, leading to

oxygen depleted hypolimnetic waters (Zander et al., 2021). Bottom water anoxia, however, is not only influenced by temperature but also by lake mixing. Holomictic mixing of the water column is suggested by high counts of Fe and Mn. The observed low abundance of APB indicators may, therefore, be explained by increased wind mixing induced by deforestation and subsequent oxygenation of bottom waters, as reported for many other small lakes (Makri et al., 2020; Sanchini et al., 2020; Tu et al., 2020; Zander et al., 2021). Forest clearance has been reported to be a primary driver of lake mixing in several small, deep lakes in Europe that can even surpass the importance of temperature variability (Sanchini et al., 2020; Zander et al., 2021).

The low presence of APB-indicators may be influenced not only by lake mixing but also by light availability. PSB, indicated by Bphe a, BChl a and okenone, are sensitive to limited light availability at the chemocline and can be negatively affected by high aquatic productivity in the epilimnion. Shading from increased productivity may reduce water transparency, thereby limiting PSB growth (Zander et al., 2023). Concentrations of pigments associated with PSB can thus even be low under permanently stratified conditions if the chemocline is situated below the photic zone (Rogozin et al., 2012). Nevertheless, under permanently stratified conditions, PSB are expected to reach higher concentrations (Gulati et al., 2017). The low abundance of APB ($RABD_{710}$ and isorenieratene) and the high counts of Fe and Mn further suggest seasonally stratified and anoxic conditions rather than permanent lake stratification with low APB concentration due to low light availability. The mixing regime can thus be described as holomictic, with at least one period of seasonal stratification.

Pigment Zone II: **Increasing anoxic conditions due to increased human impacts**

Indicators of anoxic conditions, including Bphe a cal., $RABD_{710}$, BChl a, okenone, isorenieratene and OH-spheroidene are present in low abundance. The slightly decreasing but still relatively high values in Fe and Mn, coupled with low APB pigments suggest frequent mixing and an oxygenated hypolimnion. The observed low levels of APB associated pigment concentrations are likely linked to decreasing temperatures during LIA (*Figure 16*) but may also be influenced by frequent wind mixing, as indicated in *Pigment Zone I*.

In 1950 AD, indicator pigments for anoxic conditions (BChl a, okenone, isorenieratene and OH-spheroidene) started to increase, indicating a strengthening of water column stratification and depletion of bottom water oxygenation. This first increase in APB associated pigments coincides with an increase of Fe, S and Zn. The simultaneous increase in redox-sensitive elements, high abundance of APB associated pigments and comparably low Ti count may indicate in-lake formation and deposition of iron-sulphide and zinc-sulphide minerals under anoxic conditions (Sanchini et al., 2020). Generally, in-lake formation becomes more important, as reflected in the change from positive to negative PC1 contribution (biogeochemical data). The Fe/Mn ratio follows the same pattern as the redox-sensitive elements, suggesting high bottom water oxygenation and thus presenting a contradictory pattern to the

rest of the data. Interpreting the Fe/Mn ratio in terms of bottom water oxygenation can be challenging as the elemental abundance in sediments is influenced not only by redox conditions. The sedimentary abundance of Fe and Mn is further affected by erosional input, biogeochemical processes in the water column, chemical changes in the sediment as well as hydrodynamic factors (Makri, et al., 2021). Here, the ratio is likely driven by very high Fe counts compared to Mn counts, reflecting rather the Fe content in the sediment than oxygen availability and redox conditions in the lake.

Many Swiss Plateau lakes experienced drastic increases in aquatic productivity and the onset of anoxic conditions during the mid-20th century (Makri et al., 2019, 2020; Tu et al., 2020, 2021). Even though many lakes exhibited stable stratification and hypolimnetic anoxia, they did not experience the same increase in Bphe *a* concentrations as Lake Amsoldingen. Low light availability at the chemocline due to high epilimnetic productivity may explain the low abundance of Bphe *a* in these lakes compared to Lake Amsoldingen. The high abundance of pigments associated with PSB, which are highly dependent on light availability at the chemocline, may therefore indicate permanent stratification with a stable and shallow chemocline in Lake Amsoldinge (Zander et al., 2023). Based on the findings from other Swiss Plateau lakes and elevated TC-inferred TP concentrations from 1950 AD, anoxic conditions are likely attributed to eutrophication in response to increased P inputs from the catchment.

*Pigment Zone III (*1968 to 2022 AD*):* **Modern eutrophication as a driver of bottom water anoxia**

Coinciding with the unprecedented increase in productivity in 1968 AD, anoxic conditions establish. From 2010 AD onwards (uppermost 5 cm), TChl and Bphe *a* concentrations as well as okenone and isorenieratene concentrations even show a further increase. This trend aligns with a slight increase in TC-inferred TP concentrations. Makri et al. (2020) reported a similar trend with maximum TP concentrations coinciding with highly abundant APB associated pigments. Despite the implementation of national and Europe-wide restoration programs to reduce P inputs and to counteract eutrophication in the 1980s AD, no decreasing trends in aquatic productivity and TP concentrations could be observed in Lake Amsoldingen. The lack of response to decreasing P inputs is often associated with P recycling from the sediment to the water column under anoxic and reducing conditions (Carpenter et al., 1999; Tu et al., 2020). Although TP concentrations in many Swiss Plateau lakes exhibit a lagging decrease after restoration measures (Makri et al., 2019), Lake Amsoldingen does not yet show any response in terms of aquatic productivity or TP concentrations. This aligns well with the findings of Guthruf et al. (2015), who found no improvement in P and N concentrations in the water column during the years 1993, 2003 and 2013. It has been reported that deep lakes take between 10 to 30 years to adapt to reduced nutrient conditions (Jeppesen et al., 2005; Makri et al., 2019). Anoxic conditions are not only indicated by increasing APB-associated pigments but also by low counts of Fe, Mn, S and Ca, suggesting dissolution from the sediment to the water column. *Pigment Zone III* is characterized by a sudden transition from oxygenated bottom waters to more anoxic conditions. Additionally, there is a shift from mesotrophic to eutrophic conditions, attributed to intensified agriculture.

6.3. Algal community composition

Sedimentary pigments serve as valuable tools to investigate past algal community compositions, providing information on past trophic lake states and mixing regimes (Makri et al., 2019). The measured pigment concentrations from AMS22-8 are generally very low. Previous studies showed that most pigments undergo degradation in the water column and surface sediments (Buchaca & Catalan, 2007; Leavitt, 1993; Reuss et al., 2005). The concentration of sedimented pigments is affected by various factors such as such as photo- and chemical oxidation, herbivory, as well as microbial decomposition (Buchaca & Catalan, 2007, 2008). Processes related to pigment degradation are influenced by lake morphology (lake depth, depth of oxic and photic zones, the position of the population in the water column and on lake size itself) and, therefore, differ between lakes (Buchaca & Catalan, 2007). However, pigments can undergo degradation not only in the water column or surface sediments but also post-extraction. Despite storing the pigment samples under dark, cool and oxygen-limited conditions, exposure to unfavourable conditions may still have occurred at some point in the analysis. Nevertheless, further investigation is required to understand the potential reasons for these low pigment concentrations.

Pigment Zone I: **Diatoms, dinoflagellates and chrysophytes**

Despite the low pigment concentrations, the trends in pigment compositions are rather clear. In *Pigment Zone I*, corresponding to our hypothesized MCA, oxygenic production is high. Specific carotenoids point to the dominance of diatoms, dinoflagellates and chrysophytes (diatoxanthin and fucoxanthin) within this zone. The overall co-occurring trends of chloro- and chromophyte pigments suggests that chlorophylls and their derivatives are mainly derived from these groups of phytoplankton. The relatively high and fluctuating diatom abundance is also indicated by elevated Si/Ti values. High concentrations of pigments associated with silicifying phytoplankton, such as diatoms, may be attributed to their ability to persist under nutrient-poor conditions, as they are strong competitors for P (Wetzel, 2001). P limited conditions are indicated by low TC- inferred TP concentrations in the water column. As previously discussed in Chapter 6.2., wind mixing in response to intensive deforestation plays a crucial role in regulating community composition and P availability in the water column. During holomictic seasonal mixing, oxygen from the epilimnion is transported to the hypolimnion, strengthening P retention (Tu et al., 2020). Simultaneously, P in the water column is mixed upwards, where it is available for aquatic productivity (Cohen, 2003).

Overall, phytoplankton community changes are low within this zone. The high abundance of phytoplankton species associated with diatoms, dinoflagellates and chrysophytes together with a low abundance of cyanobacteria, indicates good trophic conditions (Makri et al., 2019), which can likely be described as mesotrophic. Wind-induced mixing and the resulting distribution of oxygen and P in the water column are likely driving the trophic condition and phytoplankton community composition within

this zone. The distribution of P in the water column has been shown to play an important role in determining the composition of phytoplankton communities (Makri et al., 2019).

Pigment Zone II: **A change from low abundance to a general increase in phytoplankton**

The transition from *Pigment Zone I* to *Pigment Zone II* is marked by a decrease in chloropigments and chromophyte pigments. This overall decrease in pigment concentrations may, as previously stated, coincide with the onset of LIA (*Figure 16*) and may therefore be driven by overall colder temperatures. The low abundance of both oxygenic and anoxygenic phototrophs indicates low productivity and relatively well-oxygenated bottom waters, likely in response to wind-induced mixing. The trophic state of the lake can be described as mesotrophic, with holomictic seasonal mixing of the water column, as indicated by the low abundance of APB associated pigments (Zander et al., 2021).

Around 1933 AD to 1935 AD, the trophic state of Lake Amsoldingen was investigated for the first time, revealing mesotrophic to eutrophic conditions and well-oxygenated waters (Guthruf et al., 1999). Around 1950, an evident increase in pigment concentration may indicate a first step towards more eutrophic conditions. This change is shown by chlorophyll pigments (TChl, Chl *a*, pheophytin *a* and pheophorbide *a*), pigments associated with APB (BChl *a*, okenone, isorenieratene and OH-spheroidene) and caroteonids specific to green algae (β-carotene, lutein and zeaxanthin), diatoms, dinoflagellates (fucoxanthin, diadinoxanthin, diatoxanthin, alloxanthin) as well as cyanobacteria pigments (echinenone and canthaxanthin).

As the increase is evident across all pigments, including those that do not respond to increased nutrient inputs in subsequent periods (e.g. diatoxanthin), this trend may be explained by good pigment preservation as indicated by the low CD/TC values (Swain, 1985). The low CD/TC value, however, can also be interpreted as a change in the lakes trophic state towards more eutrophic conditions and higher cyanobacteria abundance (Guilizzoni & Lami, 2003). Thus, the peak could also be explained by a timely increase in nutrient input from the catchment. However, no specific event causing such an increase has been reported. Additionally, the increase in pigment concentrations corresponds to an increase in temperatures around the same time (*Figure 16*), suggesting temperature as an additional influencing factor. However, this does not explain why the trend is only visible in HPLC but not in the HSI data and further investigations are necessary to unravel potential reasons for this peak.

Within this zone, phytoplankton communities change substantially from overall low phytoplankton abundance towards increased concentrations of indicators of APB, green algae, diatoms, dinoflagellates and cyanobacteria. The increase in APB and cyanobacteria pigments further indicate a slight decrease in the lakes trophic state towards more eutrophic conditions. This is further shown by low CD/TC values. This change is likely explained by a combination of temperature driven community changes and higher availability of nutrients.

***Pigment Zone III* (1968 to 2022 AD)*: High phytoplankton abundance as a response to modern eutrophication**

In 1968 AD, chloropigments (TChl cal., TChl, pheophytin *a* and pheophorbide *a*), caroteonids specific to diatoms, dinoflagellates (fucoxanthin, diadinoxanthin, alloxanthin), cyanobacteria pigments (echinenone and canthaxanthin) and green algae (β-carotene, lutein and zeaxanthin) show a clear increase in their concentrations, marking the onset of modern eutrophication. The further increase in APB and cyanobacteria, together with a further decrease in the CD/TC ratio suggest a high trophic state in the lake. For the first time over the last one thousand years, the lake could be described as eutrophic. A transition to stable lake stratification and anoxic bottom water conditions in 1968 AD are indicated by increased concentrations of Bphe *a* cal., BChl *a*, okenone, isorenieratene and OH-spheroidene. Pigments associated with PSB (Bphe *a* cal, BChl *a* and okenone) further indicate the establishment of a stable and shallow chemocline (Zander et al., 2023).

As already discussed in Chapter 6.2.2., implementation measures to reduce P input into Swiss lakes did not result in decreasing aquatic productivity in Lake Amsoldingen. Even though no reduction in productivity and P concentrations could be observed, a shift in algal community composition is evident during the last 40 years in Lake Amsoldingen. The rapid growth and short life cycles of phytoplankton communities enable them to quickly adapt to changing conditions, leading to rapid changes in phytoplankton community compositions (Freeman et al., 2020). Cyanobacteria, indicated by the $RABD_{620}$ index, started to decrease around 1980 AD and reached their minimum in 2010 AD. A similar, but less pronounced trend can be seen for zeaxanthin and canthaxanthin, both associated with cyanobacteria abundance. These decreasing trends are likely linked to local protection measures such as the establishment of a nature conservation area in 1977 AD (Guthruf et al., 1999) but also to nationwide measures. A comparable shift in the phytoplankton community after the implementation of restoration programs from cyanobacteria to other phytoplankton was reported for Lake Morat (Makri et al., 2019).

TChl, Bphe *a* and $RABD_{710}$ further increased, reaching their maximum values in 2010 AD. The further strengthening of lake stratification and bottom water anoxia are also shown by okenone and isorenieratene, coinciding with the highest TC-inferred TP concentrations throughout the entire period. Under reducing conditions, P is recycled from the sediment to the water column (Tu et al., 2020). However, as the lake is in a state with strong water stratification, P is not mixed upwards and cannot be used for bio-productivity, leading to a further accumulation in the water column, altering the vertical P distribution. As reported by Makri et al. (2019), the distribution of P in the water column plays an important role in recent phytoplankton community changes.

Cyanobacteria are good competitors as they can persist under both high and low P conditions and are able to fix molecular N_2 from the atmosphere. Thus, increased temperatures, eutrophic conditions, stable stratification and low nutrient availability may favour cyanobacteria over other phytoplankton (Carey et al., 2012; Cohen, 2003; Wetzel, 2001). Cyanobacteria can even bloom under N-limited conditions and

their growth is further enhanced by additional P inputs (Smol et al., 2006). A decrease in cyanobacteria abundance may therefore further be explained by increasing N input. N is suspected to come from the grassland-dominated catchment as well as from the atmosphere in the form of wet nitrogen deposition. N emissions in Switzerland are still high, endangering different ecosystems (Seitler et al., 2016), by changing their trophic state. Wet atmospheric N deposition have been shown to promote eutrophic conditions in lakes (Bergström & Jansson, 2006). The bioavailable N is thereby not only usable for N-fixing bacteria such as cyanobacteria, but also for other phytoplankton. We therefore hypothesise that cyanobacteria may lose their competitive advantage under these high N conditions. However, not all pigments associated with cyanobacteria show the same decreasing trend. Echinenone, a pigment related to N_2-fixing cyanobacteria (Deshpande et al., 2014) remains high. However, further investigation is needed to disentangle the observed patterns.

7. Conclusions

This study aimed to investigate aquatic productivity, anoxia and sedimentary pigment dynamics in Lake Amsoldingen during the past millennium. By using a combination of high-resolution XRF and HSI data together with HPLC pigment data, we were able to reconstruct past trophic states, oxygenation of bottom waters and phytoplankton community changes. Going back to our research questions, our main findings can be summarized as follows:

    i.   How did aquatic productivity and anoxia change during the past millennium and which were the underlying causes?

During the MCA, high aquatic productivity was shown, resulting from a combination of warmer temperatures during the warm phase and increased nutrient inputs due to progressive forest clearance. In response to deforestation, the lake was subject to wind-induced mixing, preventing permanent stratification and permanent anoxic conditions in the hypolimnion. A sudden decrease in aquatic productivity could be linked to the LIA cooling around 1300 AD. Annual stratification and anoxia persisted, likely as a result of both wind-mixing and decreased temperatures. In the 1950s AD, an increase in productivity and anoxic conditions was observed, likely in response to higher nutrient inputs due to intensified agriculture. The onset of modern eutrophication, characterized by an unprecedented increase in both aquatic productivity and anoxia, is dated back to the year 1968 AD. Although a clear increase in productivity and anoxia occurred, it was less pronounced as reported for other Swiss Plateau lakes. Unlike other Swiss Plateau lakes, Lake Amsoldingen was not subject to water level lowering and drainage of the bog landscape in 1940s AD, in addition to generally more extensive agricultural practices in the catchment. These factors may explain the attenuated responses, highlighting the importance of preservation measures in mitigating the impacts of anthropogenic forcings on lakes ecosystems.

Nevertheless, eutrophication-induced stabilization of the water column led to increased anoxic conditions, enabling P recycling from the sediment, and thus further reinforces the density gradient in the water column.

ii. How does the primary productivity and anoxia history compare between pre-industrial times (before 1750 AD) and the Anthropocene (20th century)?

Aquatic productivity in pre-industrial times varied due to different forcings. During the MCA, aquatic productivity was influenced by a combination of anthropogenic and climatic impacts, whereas the decrease in productivity during LIA can be primarily attributed to lower temperatures. In the pre-industrial phase, lake bottom waters were seasonally oxygenated, as permanent stratification during times of high productivity was prevented by wind-induced vertical mixing of the water column. Around 1950 AD, a first simultaneous increase in aquatic productivity and anoxia was observed, before strongly increasing in 1968 AD, marking the onset of modern eutrophication. Such a simultaneous increase in productivity and anoxia could not be observed during the pre-industrial period, suggesting that lake stratification and, consequently, anoxia during the 20th century were further intensified by high aquatic productivity in the epilimnion. Although anthropogenic impacts substantially influenced productivity and anoxia development in both pre-industrial times and the 20th century, they differ in magnitude and impacts on the lake ecosystem. Anthropogenic impacts shifted from deforestation to more intensive agricultural practices, leading to substantial alterations in the lake's trophic state.

iii. Do changes in the pigment composition (algal communities) follow a typical succession and can this be interpreted in terms of changes in mixing regimes (nutrient availability)?

During the MCA, productivity was predominantly associated with oxygenic phototrophs such as diatoms, dinoflagellates and chrysophytes. The high presence of these species, coupled with a low abundance of cyanobacteria, indicated low trophic conditions with lower nutrient concentrations in the water column. Despite increased nutrient inputs from deforestation-related erosional inputs, wind-induced lake mixing, and subsequent bottom water oxygenation prevented phosphorus recycling and facilitated nutrient transport to the epilimnion. Consequently, community composition was likely influenced by seasonal holomictic lake mixing, facilitating nutrient distribution to the photic zone.

During the LIA, phytoplankton abundance decreased primarily due to lower temperatures. In the mid-20th century, APB, green algae, diatoms, dinoflagellates and cyanobacteria substantially increased in response to higher nutrient inputs. The concurrent presence of cyanobacteria, high

TC-inferred TP concentrations in the water column and increased bottom water anoxia indicate an increase of the lake's trophic state as a response to incomplete mixing of the water column. Elevated nutrient inputs thereby enhanced aquatic productivity, contributing to a reinforcement of lake water stratification. Under these conditions, anoxic and reducing conditions could establish, enabling P recycling from the sediment. Stratification further increased as nutrients could not be transported to the epilimnion. Phytoplankton composition followed a typical succession, with high abundance of cyanobacteria and APB during eutrophic conditions. A decline in cyanobacteria-related proxies in 1980 AD may have been attributed to an initial response to protection measures, such as the establishment of a nature protection area, or an increase in wet N-deposition from the atmosphere. Generally, changes in phytoplankton community compositions in Lake Amsoldingen can be explained by P availability and distribution in the water column influenced by lake mixing regimes.

8. Bibliography

Amann, B., Szidat, S., & Grosjean, M. (2015). A millennial-long record of warm season precipitation and flood frequency for the North-western Alps inferred from varved lake sediments: Implications for the future. *Quaternary Science Reviews*, *115*, 89–100. https://doi.org/10.1016/j.quascirev.2015.03.002

Analytical Methods Committee. (2006). Evaluation of analytical instrumentation. Part XIX CHNS elemental analysers. *Accreditation and Quality Assurance*, *11*(11), 569–576. https://doi.org/10.1007/s00769-006-0185-x

BAFU, & BLW. (2008). Umweltziele Landwirtschaft: Hergeleitet aus bestehenden rechtlichen Grundlagen. Bundesamt für Umwelt und Bundesamt für Landwirtschaft (0820; *Umwelt-Wissen*, p. 221). Bundesamt für Umwelt und Bundesamt für Landwirtschaft.

Bennett, K. D. (1996). Determination of the number of zones in a biostratigraphical sequence. *New Phytologist*, *132*(1), 155–170. https://doi.org/10.1111/j.1469-8137.1996.tb04521.x

Bergström, A.-K., & Jansson, M. (2006). Atmospheric nitrogen deposition has caused nitrogen enrichment and eutrophication of lakes in the northern hemisphere. *Global Change Biology*, *12*(4), 635–643. https://doi.org/10.1111/j.1365-2486.2006.01129.x

Bianchi, T. S., & Canuel, E. A. (2011). *Chemical Biomarkers in Aquatic Ecosystems*. Princeton University Press. https://doi.org/10.1515/9781400839100

Blankenship, R. E., & Hartman, H. (1998). The origin and evolution of oxygenic photosynthesis. *Trends in Biochemical Sciences*, *23*(3), 94–97. https://doi.org/10.1016/S0968-0004(98)01186-4

Boehrer, B., & Schultze, M. (2008). Stratification of lakes. *Reviews of Geophysics*, *46*(2). https://doi.org/10.1029/2006RG000210

Buchaca, T., & Catalan, J. (2007). Factors influencing the variability of pigments in surface sediments of mountain lakes. *Freshwater Biology*, *52(7)*, 1365–1379. https://doi.org/10.1111/j.1365-2427.2007.01774.x

Buchaca, T., & Catalan, J. (2008). On the contribution of phytoplankton and benthic biofilms to the sediment record of marker pigments in high mountain lakes. *Journal of Paleolimnology*, *40*(1), 369–383. https://doi.org/10.1007/s10933-007-9167-1

Bundesamt für Landestopografie swisstopo (n.d.). Karten der Schweiz, map.geo.admin.ch. https://map.geo.admin.ch/?lang=de&topic=ech&bgLayer=ch.swisstopo.pixelkarte-farbe&layers=ch.swisstopo.zeitreihen,ch.bfs.gebaeude_wohnungs_register,ch.bav.haltestellen-oev,ch.swisstopo.swisstlm3d-wanderwege,ch.astra.wanderland-sperrungen_umleitungen&layers_opacity=1,1,1,0.8,0.8&layers_visibility=false,false,false,false,false&layers_timestamp=18641231,,,,&E=2610548.16&N=1174854.83&zoom=9 (Last accessed 20.10.2022)

Butz, C. (2016). *Hyperspectral imaging of lake sediments: Methods and applications in a meromict lake of NE Poland*. Institute of Geography & Oeschger Centre For Climate Change Research. University of Bern, p. 225.

Butz, C., Grosjean, M., Fischer, D., Wunderle, S., Tylmann, W., & Rein, B. (2015). Hyperspectral imaging spectroscopy: A promising method for the biogeochemical analysis of lake sediments. *Journal of Applied Remote Sensing*, *9*(1), 096031. https://doi.org/10.1117/1.JRS.9.096031

Butz, C., Grosjean, M., Goslar, T., & Tylmann, W. (2017). Hyperspectral imaging of sedimentary bacterial pigments: A 1700-year history of meromixis from varved Lake Jaczno, northeast Poland. *Journal of Paleolimnology*, *58*(1), 57–72. https://doi.org/10.1007/s10933-017-9955-1

Butz, C., Grosjean, M., Poraj-Górska, A., Enters, D., & Tylmann, W. (2016). Sedimentary Bacteriopheophytin a as an indicator of meromixis in varved lake sediments of Lake Jaczno,

north-east Poland, CE 1891–2010. *Global and Planetary Change*, *144*, 109–118. https://doi.org/10.1016/j.gloplacha.2016.07.012

Carey, C. C., Ibelings, B. W., Hoffmann, E. P., Hamilton, D. P., & Brookes, J. D. (2012). Eco-physiological adaptations that favour freshwater cyanobacteria in a changing climate. *Water Research*, *46*(5), 1394–1407. https://doi.org/10.1016/j.watres.2011.12.016

Carpenter, S. R., Ludwig, D., & Brock, W. A. (1999). Management of Eutrophication for Lakes Subject to Potentially Irreversible Change. *Ecological Applications*, *9*(3), 751–771. https://doi.org/10.1890/1051-0761(1999)009[0751:MOEFLS]2.0.CO;2

Cartaxana, P., Jesus, B., & Brotas, V. (2003). Pheophorbide and pheophytin a-like pigments as useful markers for intertidal microphytobenthos grazing by Hydrobia ulvae. *Estuarine, Coastal and Shelf Science*, *58*(2), 293–297. https://doi.org/10.1016/S0272-7714(03)00081-7

Cohen, A. S. (2003). *Paleolimnology: The History and Evolution of Lake Systems*. Oxford University Press.

Correll, D. (1999). Phosphorus: A rate limiting nutrient in surface waters. *Poultry Science*, *78*(5), 674–682. https://doi.org/10.1093/ps/78.5.674

Croudace, I. W., Löwemark, L., Tjallingii, R., & Zolitschka, B. (2019). Current perspectives on the capabilities of high resolution XRF core scanners. *Quaternary International*, *514*, 5–15. https://doi.org/10.1016/j.quaint.2019.04.002

Davies, S. J., Lamb, H. F., & Roberts, S. J. (2015). Micro-XRF Core Scanning in Palaeolimnology: Recent Developments. In I. W. Croudace & R. G. Rothwell (Eds.), *Micro-XRF Studies of Sediment Cores: Applications of a non-destructive tool for the environmental sciences* (pp. 189–226). Springer Netherlands. https://doi.org/10.1007/978-94-017-9849-5_7

Dean, W. E. (1974). Determination of carbonate and organic matter in calcareous sediments and sedimentary rocks by loss on ignition; comparison with other methods. *Journal of Sedimentary Research*, *44*(1), 242–248. https://doi.org/10.1306/74D729D2-2B21-11D7-8648000102C1865D

Deshpande, B. N., Tremblay, R., Pienitz, R., & Vincent, W. F. (2014). Sedimentary pigments as indicators of cyanobacterial dynamics in a hypereutrophic lake. *Journal of Paleolimnology*, *52*(3), 171–184. https://doi.org/10.1007/s10933-014-9785-3

Eicher, U. (1987). Die spätglazialen sowie die frühpostglazialen Klimaverhältnisse im Bereiche der Alpen: Sauerstoffisotopenkurven kalkhaltiger Sedimente. *Geographica Helvetica*, *42*(2), 99–104. https://doi.org/10.5194/gh-42-99-1987

Fadeeva, V. P., Tikhova, V. D., & Nikulicheva, O. N. (2008). Elemental analysis of organic compounds with the use of automated CHNS analyzers. *Journal of Analytical Chemistry*, *63*(11), 1094–1106. https://doi.org/10.1134/S1061934808110142

Fiedor, J., Fiedor, L., Kammhuber, N., Scherz, A., & Scheer, H. (2002). Photodynamics of the Bacteriochlorophyll–Carotenoid System. 2. Influence of Central Metal, Solvent and β-Carotene on Photobleaching of Bacteriochlorophyll Derivatives¶. *Photochemistry and Photobiology*, *76*(2), 145–152. https://doi.org/10.1562/0031-8655(2002)0760145POTBCS2.0.CO2

Foley, S. F., Gronenborn, D., Andreae, M. O., Kadereit, J. W., Esper, J., Scholz, D., Pöschl, U., Jacob, D. E., Schöne, B. R., Schreg, R., Vött, A., Jordan, D., Lelieveld, J., Weller, C. G., Alt, K. W., Gaudzinski-Windheuser, S., Bruhn, K.-C., Tost, H., Sirocko, F., & Crutzen, P. J. (2013). The Palaeoanthropocene – The beginnings of anthropogenic environmental change. *Anthropocene*, *3*, 83–88. https://doi.org/10.1016/j.ancene.2013.11.002

Freeman, E. C., Creed, I. F., Jones, B., & Bergström, A.-K. (2020). Global changes may be promoting a rise in select cyanobacteria in nutrient-poor northern lakes. *Global Change Biology*, *26*(9), 4966–4987. https://doi.org/10.1111/gcb.15189

Gäggeler, H., & Szidat, S. (2016). Nuclear Dating. In F. Rösch (Ed.), Nuclear- and Radiochemistry (p. 133). De Gruyter.

Grasse, E. K., Torcasio, M. H., & Smith, A. W. (2016). Teaching UV–Vis Spectroscopy with a 3D-Printable Smartphone Spectrophotometer. *Journal of Chemical Education*, *93*(1), 146–151. https://doi.org/10.1021/acs.jchemed.5b00654

Grimm, E. C. (1987). CONISS: A FORTRAN 77 program for stratigraphically constrained cluster analysis by the method of incremental sum of squares. *Computers & Geosciences*, *13*(1), 13–35. https://doi.org/10.1016/0098-3004(87)90022-7

Gruber, N., Wehrli, B., & Wüest, A. (2000). The role of biogeochemical cycling for the formation and preservation of varved sediments in Soppensee (Switzerland). *Journal of Paleolimnology*, *24*(3), 277–291. https://doi.org/10.1023/A:1008195604287

Guilizzoni, P., & Lami, A. (2003). Paleolimnology: Use of Algal Pigments as Indicators. In *Encyclopedia of Environmental Microbiology*. John Wiley & Sons, Ltd. https://doi.org/10.1002/0471263397.env313

Guilizzoni, P., Lami, A., Marchetto, A., Jones, V., Manca, M., & Bettinetti, R. (2002). Palaeoproductivity and environmental changes during the Holocene in central Italy as recorded in two crater lakes (Albano and Nemi). *Quaternary International*, *88*(1), 57–68. https://doi.org/10.1016/S1040-6182(01)00073-8

Guilizzoni, P., Marchetto, A., Lami, A., Gerli, S., & Musazzi, S. (2011). Use of sedimentary pigments to infer past phosphorus concentration in lakes. *Journal of Paleolimnology*, *45*(4), 433–445. https://doi.org/10.1007/s10933-010-9421-9

Guthruf, J., Guthruf-Seiler, K., & Zeh, M. (1999). *Kleinseen im Kanton Bern.* Amt für Gewässerschutz und Abfallwirtschaft des Kantons Bern, Ed., Paul Haupt AG.

Guthruf, K., Maurer, V., Ryser, R., Zeh, M., & Zweifel, N. (2015). *Zustand der Kleinseen.* Bau-, Verkehrs- Und Energiedirektion Des Kantons Bern, 112.

Hamilton-Taylor, J., & Davison, W. (1995). Redox-Driven Cycling of Trace Elements in Lakes. In A. Lerman, D. M. Imboden, & J. R. Gat (Eds.), *Physics and Chemistry of Lakes* (pp. 217–263). Berlin, Heidelberg: Springer Berlin Heidelberg. https://doi.org/10.1007/978-3-642-85132-2_8

Hegerl, G. C., Brönimann, S., Cowan, T., Friedman, A. R., Hawkins, E., Iles, C., Müller, W., Schurer, A., & Undorf, S. (2019). Cause of climate change over the historical record. Environmental Research Letters, 14(12), 123006. https://doi.org/10.1088/1748-9326/ab4557

Heino, J., Alahuhta, J., Bini, L. M., Cai, Y., Heiskanen, A.-S., Hellsten, S., Kortelainen, P., Kotamäki, N., Tolonen, K. T., Vihervaara, P., Vilmi, A., & Angeler, D. G. (2021). Lakes in the era of global change: Moving beyond single-lake thinking in maintaining biodiversity and ecosystem services. *Biological Reviews*, *96*(1), 89–106. https://doi.org/10.1111/brv.12647

Heiri, O., Lotter, A. F., & Lemcke, G. (2001). Loss on ignition as a method for estimating organic and carbonate content in sediments: Reproducibility and comparability of results. *Journal of Paleolimnology*, *25*(1), 101–110. https://doi.org/10.1023/A:1008119611481

Jeffrey, S. W., & Humphrey, G. F. (1975). New spectrophotometric equations for determining chlorophylls a, b, c1 and c2 in higher plants, algae and natural phytoplankton. *Biochemie Und Physiologie Der Pflanzen*, *167*(2), 191–194. https://doi.org/10.1016/S0015-3796(17)30778-3

Jenny, J.-P., Francus, P., Normandeau, A., Lapointe, F., Perga, M.-E., Ojala, A., Schimmelmann, A., & Zolitschka, B. (2016). Global spread of hypoxia in freshwater ecosystems during the last three centuries is caused by rising local human pressure. *Global Change Biology*, *22*(4), 1481–1489. https://doi.org/10.1111/gcb.13193

Jeppesen, E., Søndergaard, M., Jensen, J. P., Havens, K. E., Anneville, O., Carvalho, L., Coveney, M. F., Deneke, R., Dokulil, M. T., Foy, B., Gerdeaux, D., Hampton, S. E., Hilt, S., Kangur, K., Köhler, J., Lammens, E. H. h. r., Lauridsen, T. L., Manca, M., Miracle, M. R., … Winder, M.

(2005). Lake responses to reduced nutrient loading – an analysis of contemporary long-term data from 35 case studies. *Freshwater Biology*, *50*(10), 1747–1771. https://doi.org/10.1111/j.1365-2427.2005.01415.x

Juillot, F., Noël, V., Louvat, P., Gelabert, A., Jouvin, D., Göttlicher, J., Belin, S., Müller, B., Morin, G., & Voegelin, A. (2023). Can Zn isotopes in sediments record past eutrophication of freshwater lakes? A pilot study at Lake Baldegg (Switzerland). *Chemical Geology*, *620*, 121321. https://doi.org/10.1016/j.chemgeo.2023.121321

Lami, A., Guilizzoni, P., & Marchetto, A. (2000). High resolution analysis of fossil pigments, carbon, nitrogen and sulphur in the sediment of eight European Alpine lakes: The MOLAR project. *Journal of Limnology*, *59(1)*, 15–28. https://doi.org/10.4081/jlimnol.2000.s1.15

Last, W. M., & Smol, J. P. (2002). *Tracking Environmental Change Using Lake Sediments: Volume 1: Basin Analysis, Coring, and Chronological Techniques.* Developments in Paleoenvironmental Research, pp. 573. Dordrecht:Springer Netherlands. //www.springer.com/de/book/9781402006289.

Leavitt, P. R. (1993). A review of factors that regulate carotenoid and chlorophyll deposition and fossil pigment abundance. *Journal of Paleolimnology*, *9*(2), 109–127. https://doi.org/10.1007/BF00677513

Leavitt, P. R., & Hodgson, D. A. (2001). 'Sedimentary Pigments'. *In Tracking Environmental Change Using Lake Sediments: Terrestrial, Algal, and Siliceous Indicators*, edited by John P. Smol, H. John B. Birks, William M. Last, Raymond S. Bradley, and Keith Alverson, 295–325. Developments in Paleoenvironmental Research. Dordrecht: Springer Netherlands. https://doi.org/10.1007/0-306-47668-1_15.

Lee, M., Shevliakova, E., Malyshev, S., Milly, P. C. D., & Jaffé, P. R. (2016). Climate variability and extremes, interacting with nitrogen storage, amplify eutrophication risk. *Geophysical Research Letters*, *43*(14), 7520–7528. https://doi.org/10.1002/2016GL069254

Li, J., Xiao, X., Xian, X., Li, S., Yu, X., & Zhang, X. (2023). Green algae outcompete cyanobacteria in a shallow lake, Longhu Lake. *Water Supply*, *23*(7), 2649–2661. https://doi.org/10.2166/ws.2023.154

Liu, B., Chen, S., Liu, H., & Guan, Y. (2020). Changes in the ratio of benthic to planktonic diatoms to eutrophication status of Muskegon Lake through time: Implications for a valuable indicator on water quality. *Ecological Indicators*, *114*, 106284. https://doi.org/10.1016/j.ecolind.2020.106284

Lotter, A., & Boucherle, M. M. (1984). A late-glacial and post-glacial history of Amsoldingersee and vicinity, Switzerland. *Schweizerische Zeitschrift für Hydrologie*, *46*(2), 192–209. https://doi.org/10.1007/BF02538061

Lotter, A. F. (2001). The palaeolimnology of Soppensee (Central Switzerland), as evidenced by diatom, pollen, and fossil-pigment analyses. *Journal of Paleolimnology*, *25*(1), 65–79. https://doi.org/10.1023/A:1008140122230

Luterbacher, J., Dietrich, D., Xoplaki, E., Grosjean, M., & Wanner, H. (2004). European Seasonal and Annual Temperature Variability, Trends,and Extremes Since 1500. *Science 303*(5663), 1499–1503. https://doi.org/10.1126/science.1093877

Luterbacher, J., Werner, J. P., Smerdon, J. E., Fernández-Donado, L., González-Rouco, F. J., Barriopedro, D., Ljungqvist, F. C., Büntgen, U., Zorita, E., Wagner, S., Esper, J., McCarroll, D., Toreti, A., Frank, D., Jungclaus, J. H., Barriendos, M., Bertolin, C., Bothe, O., Brázdil, R., Camuffo, O., Dobrovolný, P., Gagen, M., García-Bustamante, E., Ge, Q., Gómez-Navarro, J. J., Guiot, J., Hao, Z., Hegerl, G. C., Holmgren, K., Klimenko, V. V., Martín-Chivelet, J., Pfister, C., Roberts, N., Schindler, A., Schurer, A., Solomina, O., von Gunten, L., Wahl, E., Wanner, H., Wetter, O., Xoplaki, E., Yuan, N., Zanchettin, D., Zhang, H., Zerefos, C. (2016).

European summer temperatures since Roman times. *Environmental Research Letters*, *11*(2), 024001. https://doi.org/10.1088/1748-9326/11/2/024001

Makri, S., Lami, A., Lods-Crozet, B., & Loizeau, J.-L. (2019). Reconstruction of trophic state shifts over the past 90 years in a eutrophicated lake in western Switzerland, inferred from the sedimentary record of photosynthetic pigments. *Journal of Paleolimnology*, *61*(2), 129–145. https://doi.org/10.1007/s10933-018-0049-5

Makri, S., Rey, F., Gobet, E., Gilli, A., Tinner, W., & Grosjean, M. (2020). Early human impact in a 15,000-year high-resolution hyperspectral imaging record of paleoproduction and anoxia from a varved lake in Switzerland. *Quaternary Science Reviews*, *239*, 106335. https://doi.org/10.1016/j.quascirev.2020.106335

Makri, S., Wienhues, G., Bigalke, M., Gilli, A., Rey, F., Tinner, W., Vogel, H., & Grosjean, M. (2021). Variations of sedimentary Fe and Mn fractions under changing lake mixing regimes, oxygenation and land surface processes during Late-glacial and Holocene times. *Science of The Total Environment*, *755*, 143418. https://doi.org/10.1016/j.scitotenv.2020.143418

Meyers, P. A., and J. L. Teranes. (2001). "Sediment Organic Matter". In *Tracking Environmental Change Using Lake Sediments: Volume 2: Physical and Geochemical Methods*, edited by William M. Last and John P. Smol, 239-270. Developments in Paleoenvironmental Research. Dordrecht: Springer Netherlands.

Myrbo, A., Morrison, A., & McEwan, R. (2011). Tool for Microscopic Identification (TMI). http://tmi.laccore.umn.edu, last accessed 20.10.2023.

Ohlendorf, C., Wennrich, V., & Enters, D. (2015). 'Experiences with XRF-Scanning of Long Sediment Records'. In I. W. Croudace & R. G. Rothwell (Eds.), *Micro-XRF Studies of Sediment Cores: Applications of a non-destructive tool for the environmental sciences* (pp. 351–372). Springer Netherlands. https://doi.org/10.1007/978-94-017-9849-5_13

Pfister, C., & Wanner, H. (2021). *Climate and Society in Europe: The Last Thousand Years*. Haupt Verlag, 2021.

R Core Team. (2022). R: A language and environment for statistical computing. https://www.R-project.org/. R Foundation for Statistical Computing.

Reuss, N., Conley, D. J., & Bianchi, T. S. (2005). Preservation conditions and the use of sediment pigments as a tool for recent ecological reconstruction in four Northern European estuaries. *Marine Chemistry*, *95*(3), 283–302. https://doi.org/10.1016/j.marchem.2004.10.002

Rogozin, D. Yu., Zykov, V. V., & Degermendzhi, A. G. (2012). Ecology of purple sulfur bacteria in the highly stratified meromictic Lake Shunet (Siberia, Khakassia) in 2002–2009. *Microbiology*, *81*(6), 727–735. https://doi.org/10.1134/S0026261712060148

Rousseeuw, P. J. (1987). Silhouettes: A graphical aid to the interpretation and validation of cluster analysis. *Journal of Computational and Applied Mathematics*, *20*, 53–65. https://doi.org/10.1016/0377-0427(87)90125-7

Sahu, P. K., Ramisetti, N. R., Cecchi, T., Swain, S., Patro, C. S., & Panda, J. (2018). An overview of experimental designs in HPLC method development and validation. *Journal of Pharmaceutical and Biomedical Analysis*, *147*, 590–611. https://doi.org/10.1016/j.jpba.2017.05.006

Sanchini, A., & Grosjean, M. (2020). Quantification of chlorophyll a, chlorophyll b and pheopigments a in lake sediments through deconvolution of bulk UV–VIS absorption spectra. *Journal of Paleolimnology*, *64*(3), 243–256. https://doi.org/10.1007/s10933-020-00135-z

Sanchini, A., Szidat, S., Tylmann, W., Vogel, H., Wacnik, A., & Grosjean, M. (2020). A Holocene high-resolution record of aquatic productivity, seasonal anoxia and meromixis from varved sediments of Lake Łazduny, North-Eastern Poland: Insight from a novel multi-proxy approach. *Journal of Quaternary Science*, *35*(8), 1070–1080. https://doi.org/10.1002/jqs.3242

Santisteban, J. I., Mediavilla, R., López-Pamo, E., Dabrio, C. J., Zapata, M. B. R., García, M. J. G., Castaño, S., & Martínez-Alfaro, P. E. (2004). Loss on ignition: A qualitative or quantitative method for organic matter and carbonate mineral content in sediments? *Journal of Paleolimnology*, *32*(3), 287–299. https://doi.org/10.1023/B:JOPL.0000042999.30131.5b

Schlegel, I., Koschel, R., & Krienitz, L. (1998). On the occurrence of Phacotus lenticularis (Chlorophyta) in lakes of different trophic state. In M. Alvarez-Cobelas, C. S. Reynolds, P. Sánchez-Castillo, & J. Kristiansen (Eds.), *Phytoplankton and Trophic Gradients* (pp. 353–361). Springer Netherlands. https://doi.org/10.1007/978-94-017-2668-9_30

Schnurrenberger, D., Russell, J., & Kelts, K. (2003). Classification of lacustrine sediments based on sedimentary components. *Journal of Paleolimnology*, *29*(2), 141–154. https://doi.org/10.1023/A:1023270324800

Seitler, E., Thöni, L., & Meier, M. (2016). Atmosphärische Stickstoff-Deposition in der Schweiz 2000 bis 2014 (p. 105). *FUB – Forschungsstelle für Umweltbeobachtung*, *Rapperswil*.

Shapley, M. D., Ito, E., & Donovan, J. J. (2005). Authigenic calcium carbonate flux in groundwater-controlled lakes: Implications for lacustrine paleoclimate records. *Geochimica et Cosmochimica Acta*, *69*(10), 2517–2533. https://doi.org/10.1016/j.gca.2004.12.001

Smol, J., Birks, H., Last, W., Bradley, R., & Alverson, K. (2001). *Tracking Environmental Change Using Lake Sediments: Terrestrial, Algal, and Siliceous Indicators.* Developments in Paleoenvironmental Research, pp. 371. Dordrecht: Springer Netherlands. https://doi.org/10.1007/0-306-47668-1

Sorrel, P., Jacq, K., Van Exem, A., Escarguel, G., Dietre, B., Debret, M., McGowan, S., Ducept, J., Gauthier, E., & Oberhänsli, H. (2021). Evidence for centennial-scale Mid-Holocene episodes of hypolimnetic anoxia in a high-altitude lake system from central Tian Shan (Kyrgyzstan). *Quaternary Science Reviews*, *252*, 106748. https://doi.org/10.1016/j.quascirev.2020.106748

Swain, E. B. (1985). Measurement and interpretation of sedimentary pigments. *Freshwater Biology*, *15*(1), 53–75. https://doi.org/10.1111/j.1365-2427.1985.tb00696.x

Swarzenski, P. W. (2014). 210Pb Dating. In W. J. Rink & J. Thompson (Eds.), *Encyclopedia of Scientific Dating Methods* (pp. 1–11). Springer Netherlands. https://doi.org/10.1007/978-94-007-6326-5_236-1

Thorndike, R. L. (1953). Who belongs in the family? *Psychometrika*, *18*(4), 267–276. https://doi.org/10.1007/BF02289263

Tu, L., Gilli, A., Lotter, A. F., Vogel, H., Moyle, M., Boyle, J. F., & Grosjean, M. (2021). The nexus among long-term changes in lake primary productivity, deep-water anoxia, and internal phosphorus loading, explored through analysis of a 15,000-year varved sediment record. *Global and Planetary Change*, *207*, 103643. https://doi.org/10.1016/j.gloplacha.2021.103643

Tu, L., Zander, P., Szidat, S., Lloren, R., & Grosjean, M. (2020). The influences of historic lake trophy and mixing regime changes on long-term phosphorus fraction retention in sediments of deep eutrophic lakes: A case study from Lake Burgäschi, Switzerland. *Biogeosciences*, *17*(10), 2715–2729. https://doi.org/10.5194/bg-17-2715-2020

Tylmann, W., Fischer, H. W., Enters, D., Kinder, M., Moska, P., Ohlendorf, C., Poręba, G., & Zolitschka, B. (2014). Reply to the comment by F. Gharbi on 'Multiple dating of varved sediments from Lake Łazduny, northern Poland: Toward an improved chronology for the last 150 years'. *Quaternary Geochronology*, *20*, 111–113. https://doi.org/10.1016/j.quageo.2013.04.003

Vinçon-Leite, B., & Casenave, C. (2019). Modelling eutrophication in lake ecosystems: A review. *Science of The Total Environment*, *651*, 2985–3001. https://doi.org/10.1016/j.scitotenv.2018.09.320

Weltje, G. J., & Tjallingii, R. (2008). Calibration of XRF core scanners for quantitative geochemical logging of sediment cores: Theory and application. *Earth and Planetary Science Letters*, *274*(3), 423–438. https://doi.org/10.1016/j.epsl.2008.07.054

Wetzel, R. G. (2001). *Limnology: Lake and River Ecosystems*. 3rd ed. San Diego: Gulf Professional Publishing.

Zander, P. D., Wienhues, G., & Grosjean, M. (2022). Scanning Hyperspectral Imaging for In Situ Biogeochemical Analysis of Lake Sediment Cores: Review of Recent Developments. *Journal of Imaging*, *8*(3), 58. https://doi.org/10.3390/jimaging8030058

Zander, P. D., Wirth, S. B., Gilli, A., Peduzzi, S., & Grosjean, M. (2023). Hyperspectral imaging sediment core scanning tracks high-resolution Holocene variations in (an)oxygenic phototrophic communities at Lake Cadagno, Swiss Alps. *Biogeosciences*, *20*(12), 2221–2235. https://doi.org/10.5194/bg-20-2221-2023

Zander, P. D., Żarczyński, M., Vogel, H., Tylmann, W., Wacnik, A., Sanchini, A., & Grosjean, M. (2021). A high-resolution record of Holocene primary productivity and water-column mixing from the varved sediments of Lake Żabińskie, Poland. *Science of The Total Environment*, *755*, 143713. https://doi.org/10.1016/j.scitotenv.2020.143713

Zolitschka, B., Francus, P., Ojala, A. E. K., & Schimmelmann, A. (2015). Varves in lake sediments – a review. *Quaternary Science Reviews*, *117*, 1–41. https://doi.org/10.1016/j.quascirev.2015.03.019

Züllig, H. (1986). Carotenoids from plankton and photosynthetic bacteria in sediments as indicators of trophic changes in Lake Lobsigen during the last 14000 years. *Hydrobiologia*, *143*(1), 315–319. https://doi.org/10.1007/BF00026676

9. Appendix

9.1. XRF data
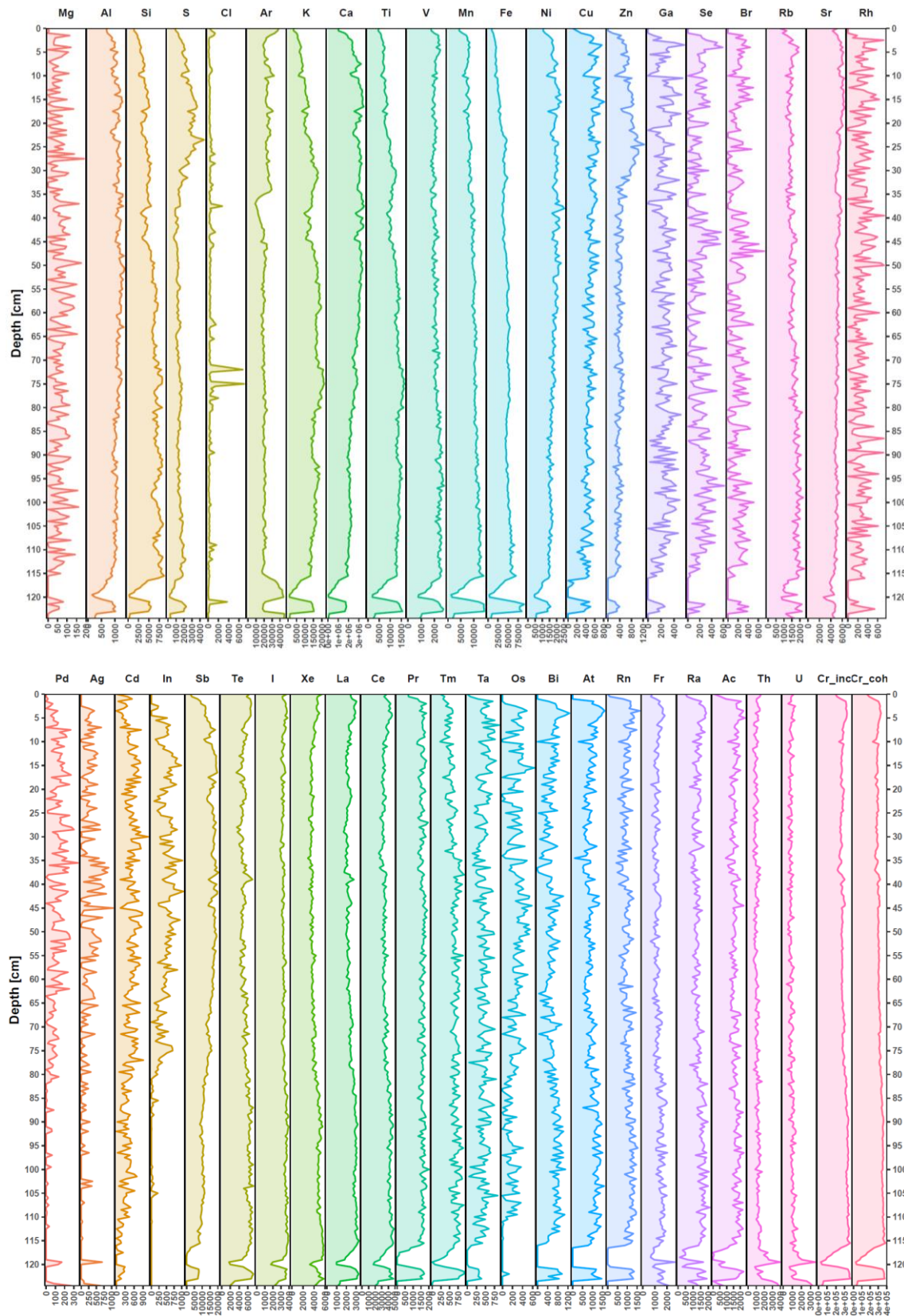
Figure A1: *Overview over all XRF-measurements from AMS22-8. The data is plotted related to depth and given in counts per second [cps].*
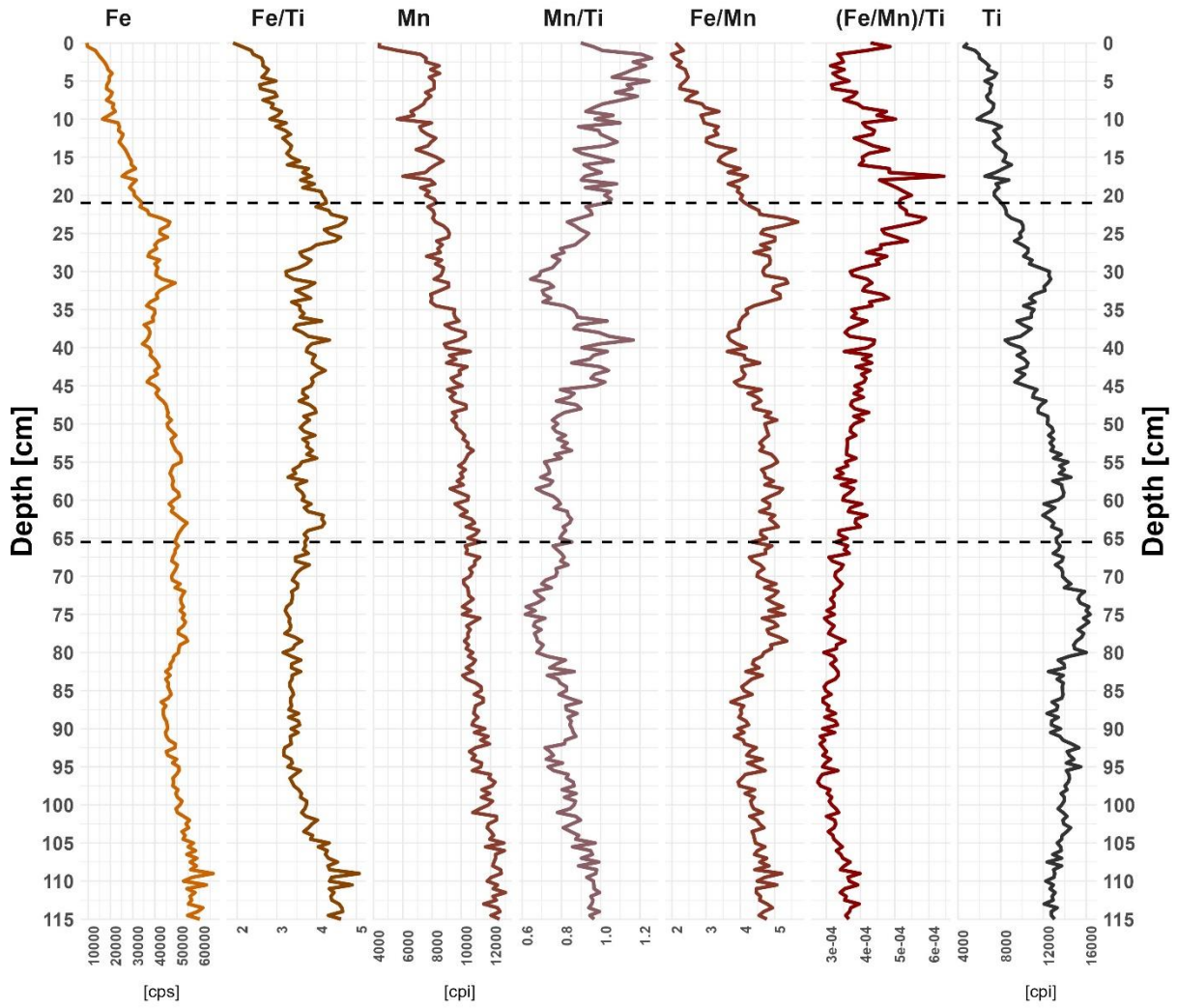
Figure A2: Selected XRF measurements divided by Ti counts, measured from AMS22-8.

9.2. HIS data

9.2.1 Spectral indices

Definitions of the different HSI indices are given in *Equations (A1 – A4):*

$$RABD_{673} = \frac{\dfrac{21 \times R_{640.28} + 23 \times R_{709.95}}{21 + 23}}{R_{673}}$$

(A1)

$$RABD_{845} = \frac{\dfrac{34 \times R_{790.26} + 34 \times R_{899.64}}{34 + 34}}{R_{845}}$$

(A2)

$$RABD_{710} = \frac{\dfrac{13 \times R_{689.28} + 13 \times R_{730.66}}{13 + 13}}{R_{710}}$$

<div align="right">

(A3)

</div>

$$RABD_{620} = \frac{\dfrac{19 \times R_{590.2} + 19 \times R_{649.73}}{19 + 19}}{R_{620}}$$

<div align="right">

(A4)

</div>

9.2.1 HSI data
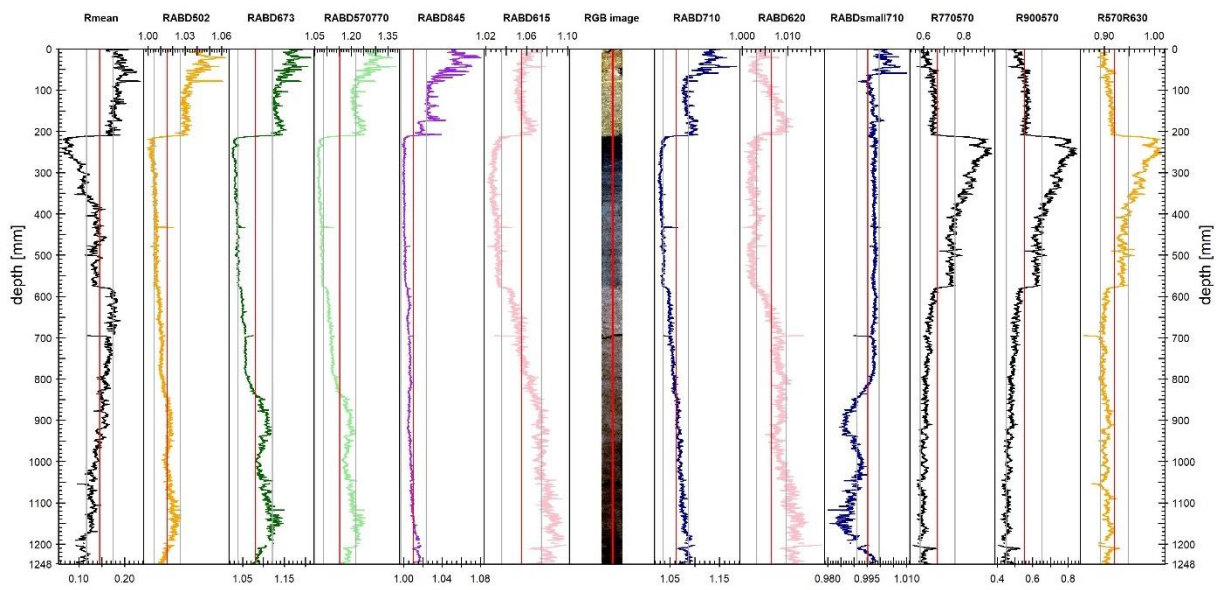
Figure A3: *Spectral indices measured with HSI from AMS22-8.*

9.3. HPLC data
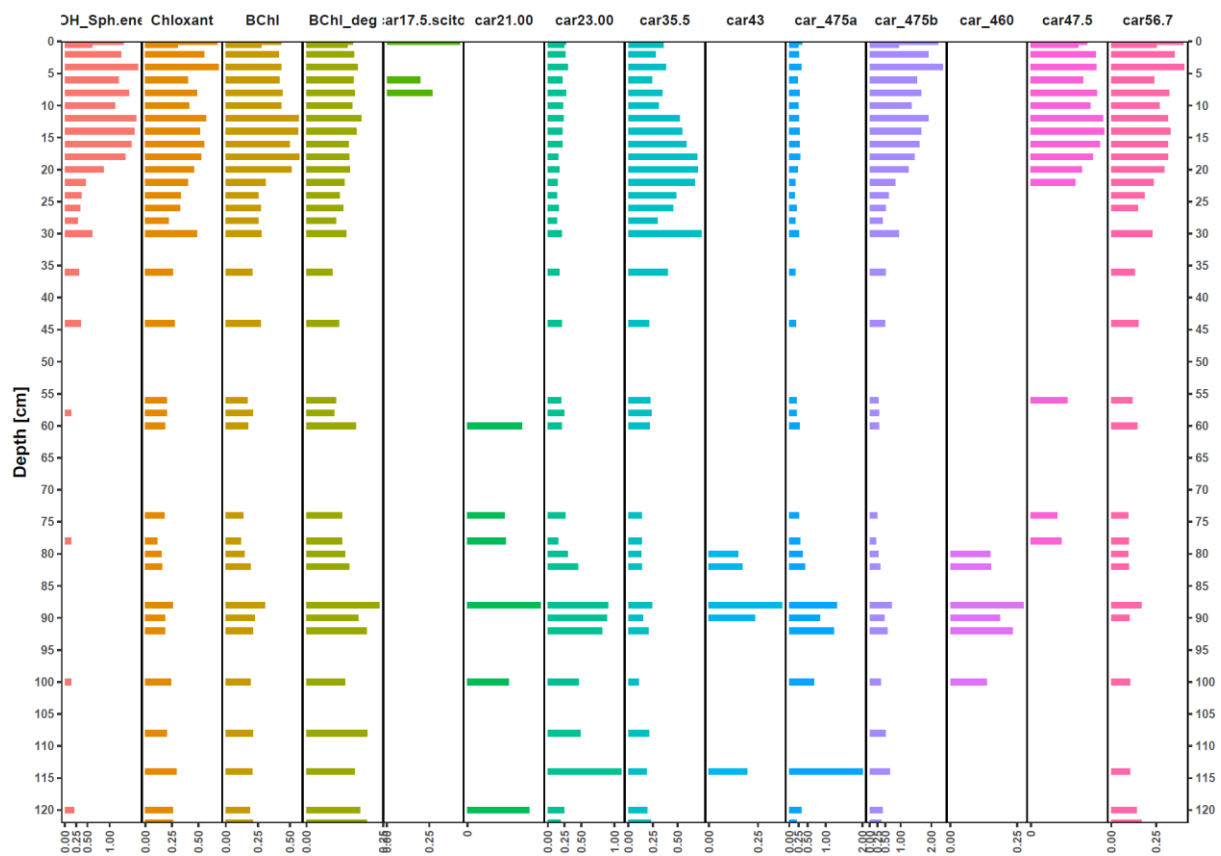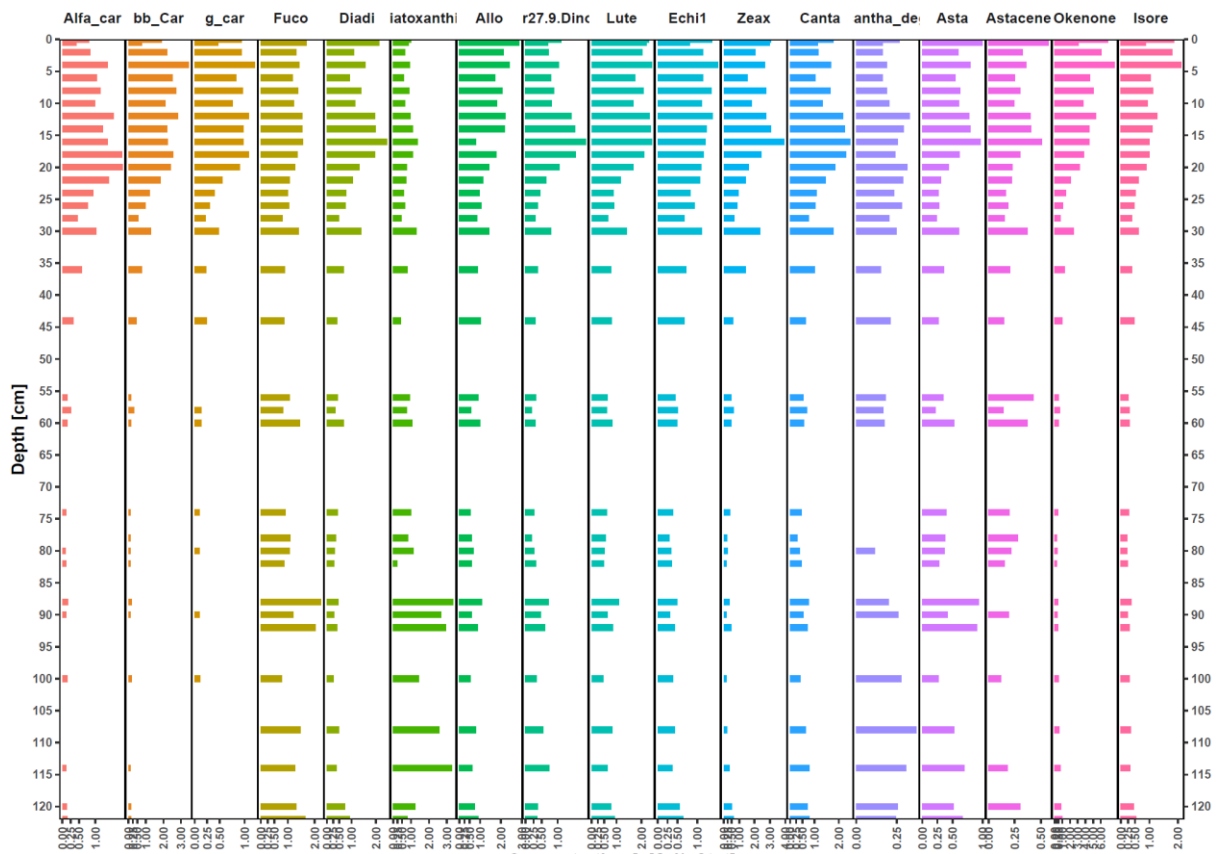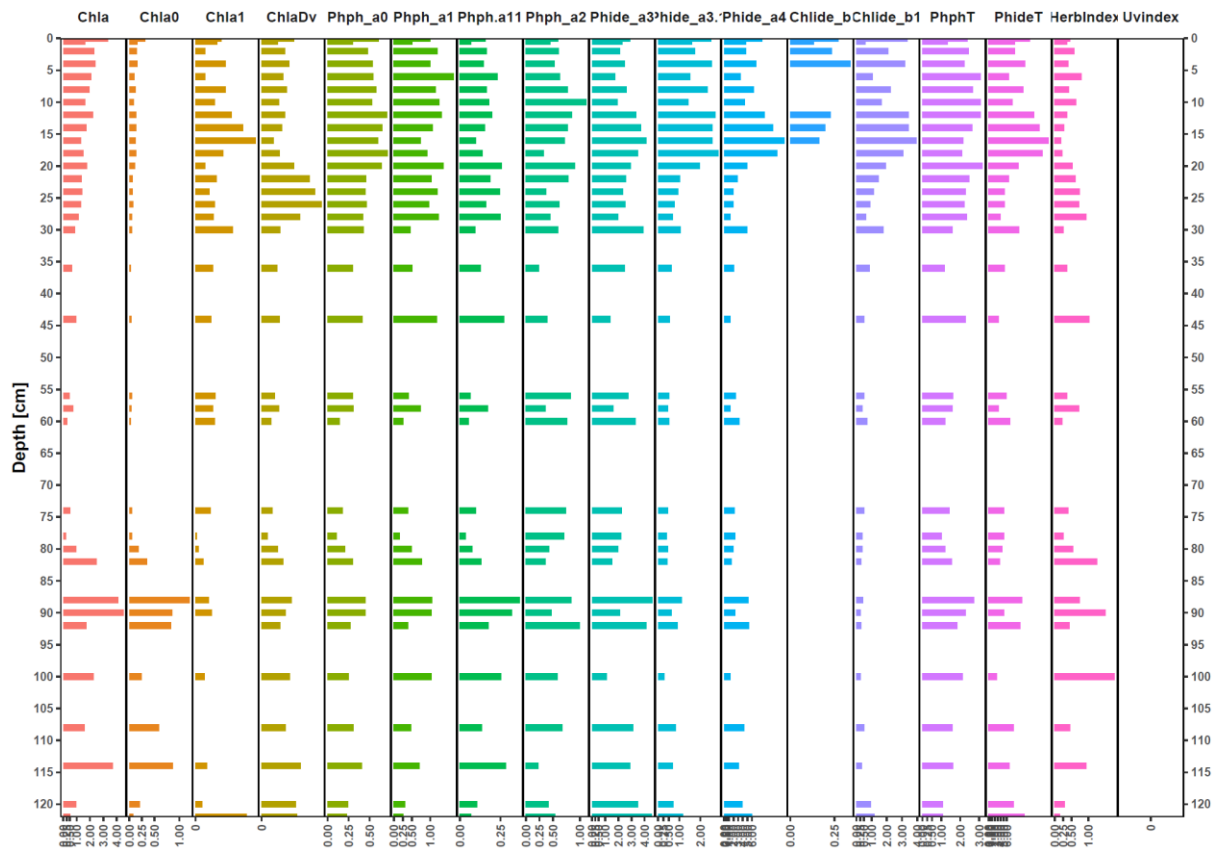
Figure A4: *HPLC derived pigment concentrations given in [nmol/g wet sediment] from AMS22-8.*

10. Acknowledgements

11. Declaration of consent

Declaration of consent

on the basis of Article 30 of the RSL Phil.-nat. 18

Name/First Name: Ogi Sarah Lea

Registration Number: 18-109-447

Study program: Masters in Climate Sciences

Bachelor ☐   Master ☑   Dissertation ☐

Title of the thesis: Aquatic productivity, anoxia and sedimentary pigment dynamics in Lake Amsoldingen in the past Millennium

Supervisor: Prof. Dr. Martin Grosjean
Dr. Petra Zahajská

I declare herewith that this thesis is my own work and that I have not used any sources other than those stated. I have indicated the adoption of quotations as well as thoughts taken from other authors as such in the thesis. I am aware that the Senate pursuant to Article 36 paragraph 1 litera r of the University Act of 5 September, 1996 is authorized to revoke the title awarded on the basis of this thesis.

For the purposes of evaluation and verification of compliance with the declaration of originality and the regulations governing plagiarism, I hereby grant the University of Bern the right to process my personal data and to perform the acts of use this requires, in particular, to reproduce the written thesis and to store it permanently in a database, and to use said database, or to make said database available, to enable comparison with future theses submitted by others.

Bern, 06.01.2024
Place/Date

Signature